Available online at www.sciencedirect.com

SciVerse ScienceDirect

Geochimica et Cosmochimica Acta 80 (2012) 30–50

Geochimica et Cosmochimica Acta

www.elsevier.com/locate/gca

Effect of the heterotrophic bacterium *Pseudomonas reactans* on olivine dissolution kinetics and implications for CO_2 storage in basalts

L.S. Shirokova [a,b], P. Bénézeth [a], O.S. Pokrovsky [a,*], E. Gerard [c], B. Ménez [c], H. Alfredsson [d]

[a] *Géochimie et Biogéochimie Expérimentale, Géosciences Environnement Toulouse (GET), UMR 5563, CNRS, Université de Toulouse, 14 Avenue Edouard Belin, 31400 Toulouse, France*

[b] *Institute of Ecological Problems of the North, 23 Nab. Severnoy Dviny, Russian Academy of Science, Arkhangelsk, Russia*

[c] *Institut de Physique du Globe de Paris, 1 rue Jussieu, 75238 Paris, France*

[d] *University of Iceland, Sudurgata, IS 101 Reykjavík, Iceland*

Received 1 February 2011; accepted in revised form 29 November 2011; available online 7 December 2011

Abstract

This work is aimed at quantification of forsteritic olivine (Fo_{92}) dissolution kinetics in batch and mixed-flow reactors in the presence of aerobic gram-negative bacteria (*Pseudomonas reactans* HK 31.3) isolated from an instrumented well located within a basaltic aquifer in Iceland. The release rate of mineral constituents was measured as a function of time in the presence of live and dead cells in constant-pH (4–9), bicarbonate-buffered (0.001–0.05 M), nutrient-rich and nutrient-free media in batch reactors at 0–30 atm of CO_2 partial pressure (pCO_2). In batch reactors at 30 atm pCO_2, 0.1 M NaCl and 0.05 M $NaHCO_3$ the rates were weakly affected by the presence of bacteria. In nutrient media, the SEM observation of reacted grains revealed the presence of biofilm-like surface coverage that does not modify Mg and Si release rate at the earlier stages of reaction but significantly decreased the dissolution after prolonged exposure.

Olivine dissolution rates measured in flow-through reactors are not affected by the presence of dead and live bacteria at pH $\geqslant$9 in 0.01 M $NaHCO_3$ solutions. In circumneutral, CO_2-free solutions at pH close to 6, both live and dead bacteria increase the dissolution rate, probably due to surface complexation of exudates and lysis products. In most studied conditions, the dissolution was stoichiometric with respect to Mg and Si release and no formation of secondary phases was evidenced by microscopic examination of post-reacted grains. Obtained results are consistent with known molecular mechanism of olivine dissolution and its surface chemistry. Overall, this work demonstrates negligible effect of *P. reactans* on olivine reactivity under conditions of CO_2 storage in the wide range of aqueous fluid composition.

1. INTRODUCTION

Quantification of the effect of microorganisms and associated organic ligands on mineral dissolution rate is one among the last remaining challenges in modeling water–rock interactions under the Earth surface and in subsurface environments. This is especially true for underground settings within the context of CO_2 capture, sequestration and storage. First, elevated CO_2 partial pressures (pCO_2) create numerous experimental difficulties for performing robust flow-through experiments at a given saturation state. Second, despite several recent works aimed at characterizing silicate mineral dissolution under elevated pCO_2 (e.g., Giammar et al., 2005; Bearat et al., 2006; Sorai et al., 2007; Daval et al., 2009, 2010; Hangx and Spiers, 2009;

* Corresponding author.
E-mail address: oleg@get.obs-mip.fr (O.S. Pokrovsky).

0016-7037/$ - see front matter © 2011 Elsevier Ltd. All rights reserved.
doi:10.1016/j.gca.2011.11.046

Matter and Kelemen, 2009; Garcia et al., 2010), the reactivity of main rock-forming minerals even in abiotic systems at $pCO_2 >> 1$ atm and circumneutral pH is still poorly constrained. And third, most of bacterial species of the subsurface biosphere habitats are difficult to culture in the laboratory, many bacteria and archaea cultures can live only as consortium of microorganisms which is very hard to maintain at a controlled and stable biomass concentration and there is still a very limited number of characterizations of the communities of microbes present in subsurface environments. In this regard, experiments with cultures separated from real natural settings and using well-defined mineral substrate, whose reaction mechanism is known, are very timing.

Forsteritic olivine (Fo_{92}, San Carlos) was chosen as typical and representative mineral of mafic and ultramafic rocks, widely considered in carbon dioxide mineral sequestration mechanisms. Numerous studies have been devoted to the dissolution kinetics of forsterite (Luce et al., 1972; Sanemasa et al., 1972; Grandstaff, 1978, 1986; Siever and Woodford, 1979; Eriksson, 1982; Sverdrup and Bjerle, 1982; Schott and Berner, 1983; Siegel and Pfannkuch, 1984, 1985; Murphy and Helgeson, 1987; Blum and Lasaga, 1988; Sverdrup, 1990; Wogelius and Walther, 1991, 1992; Westrich et al., 1993; Awad et al., 2000; Chen and Brantley, 2000; Rosso and Rimstidt, 2000; Pokrovsky and Schott, 2000b; Oelkers, 2001). In these studies, it has been recognized that at 25 °C and $pH < 7$, forsterite dissolves congruently and the rate is proportional to the activity of protons. In alkaline solutions at pH above 8, the rate was found to be pH-independent in CO_2-free solutions and decreasing by 1–1.5 order of magnitude in $NaHCO_3$ or Na_2CO_3-bearing solutions. Recently, renewed interest to olivine dissolution was stimulated due to the use of this mineral for in situ and ex-situ carbon dioxide sequestration via mineral carbonation reactions (Giammar et al., 2005; Bearat et al., 2006; Hänchen et al., 2006, 2007; Prigiobbe et al., 2009a,b). However, kinetics of olivine dissolution in CO_2-bearing solutions remains poorly quantified and, to the best of our knowledge, nothing is known on the forsterite dissolution at elevated pCO_2 in the presence of microorganisms.

Numerous laboratory and field studies indicate that bacteria can significantly affect aluminosilicates and Al, Fe oxides dissolution rates at the earth-surface conditions (Bennett and Casey, 1994; Vandevivere et al., 1994; Welch and Vandevivere, 1994; Grantham et al., 1997; Edwards et al., 2004). Whereas bacterial exometabolites and lysis products are capable of complexing Al^{3+} at the mineral surface and in aqueous solution thus facilitating the breaking of Al–O bonds or decreasing the saturation state of the system, the exopolysaccharides (EPS) may as well inhibit dissolution rates by blocking the mineral surface cation detachment sites (Lee and Fein, 2000). Much less is known on the effect of bacteria on "basic" Ca, Mg-bearing silicate dissolution rates. Unlike aluminosilicates, olivine is not affected by the chemical affinity and metal complexation in solution, so the effect of organic matter should be weaker. In a series of laboratory experiments, we demonstrated that the effect of a wide range of organic ligands, comprising both carboxylic acids and analogs of cell exometabolites on the overall dissolution rate of brucite ($Mg(OH)_2$), wollastonite ($CaSiO_3$), diopside ($CaMgSi_2O_6$) and di-octahedric smectite (Al-bearing clay) at the conditions of interstitial soil solutions is negligible compared to that of solution pH (Pokrovsky et al., 2005; Golubev and Pokrovsky, 2006; Golubev et al., 2006). However, the main difficulty of quantifying the effect of bacteria on mineral dissolution in laboratory experiments is that the change of pH value during microbial growth and metabolism may have significant impact on overall mineral reactivity as was often observed in earlier (Kutuzova, 1969; Lebedeva et al., 1979; Malinovskaya et al., 1990) and later (Wu et al., 2007, 2008) studies. The use of inorganic buffer such as phosphate (e.g., Hutchens et al., 2003) does not allow straightforward mineral rate interpretation because orthophosphate at $pH = 7$ is known to significantly accelerate mineral dissolution (Pokrovsky et al., 2005a, 2009b); as a results, microbe (organic) ligand–phosphate competition may occur.

The motivation for this work is to quantitatively access the effect of microbial activity on olivine dissolution. There are several recent studies dealing with quantifying the effect of bacteria on basalt and granite rock dissolution (Wu et al., 2007, 2008). However, due to the complexity of the whole rock systems, assessing the elementary mechanisms that control the element release in mineral–bacteria system from available data is rather difficult. From the other hand, extensive studies on aluminosilicates (Bennett and Casey, 1994; Barker et al., 1997) and calcite (Friis et al., 2003; Lüttge and Conrad, 2004; Davis et al., 2007) dissolution in the presence of bacteria cannot be directly applied to basic silicates including forsterite because of different reaction mechanisms involved in these interactions.

To provide a better understanding of bacteria–mineral interaction in the context of CO_2 geological storage, we selected a common soil and underground bacterium, *Pseudomonas reactans.* Bacterial strain of genera *Pseudomonas*, thanks to their relatively easy culturing, have been frequently used as a model organism in studying mineral weathering in the past (i.e., Webley et al., 1960, 1963; Duff et al., 1962) and recently (Pokrovsky et al., 2009a,b). Although culturable bacteria may only represent a small proportion of the species present in natural settings (e.g., Pedrós-Alió, 2006), they still remain the best candidates for rigorous quantification of mineral dissolution rates both in closed and open-system reactors.

The main actions of bacteria with respect to forsterite dissolution are: (1) adsorbing to mineral surface thus polarizing the bonds; (2) producing exometabolites and lysis products, thus changing the speciation in solution and the saturation state; (3) creating a proton flux from the cell cytoplasm through the cell wall to the aqueous environment thus increasing the acidity of the system (Urrutia Mera et al., 1992); (4) assimilating released mineral components in the interior of the cells via irreversible reaction; (5) adsorbing the dissolution products on the cell surface via reversible reaction. Altogether, these parallel and consecutive processes produce four main sink of mineral constituents (e.g., Mg, Si) after their release from the mineral structure: (i) adsorbed at the cell surface; (ii) incorporated

inside the cells; (iii) complexed with cell exometabolites and lysis products in aqueous solution and (iv) present in the form of aqueous ions, neutral molecules or simple complexes. In this work, we attempted quantifying the relative contribution of each of these processes to the overall rate of Si and Mg release from the olivine surface in order to separate the short-term effect of bacterial presence (adsorption and assimilation in the course of cell growth) from the long-term mineral dissolution and precipitation reactions, most important for elaborating robust CO_2 sequestration scenarios. Towards this goal, we conducted a series of rigorously designed experiments in batch and flow-through reactors under constant biomass concentration, in the presence of both live and dead (inactivated) bacteria in the nutrient-free and nutrient- bearing media with and without mineral.

2. MATERIALS AND METHODS

2.1. Mineral, solutions and analyses

Forsterite from San Carlos (Arizona) was used in this study. The chemical analysis of this sample is given in Pokrovsky and Schott (2000a) and corresponds to the composition $Mg_{1.82}Fe_{0.18}SiO_4$ (Fo_{92}). X-ray diffraction analysis of this material before and after experiments revealed neither contamination by clay minerals nor the formation of secondary phases. Transparent crystals ~0.5 cm in size were hand-picked, ground with an agate mortar and pestle, and sieved. Two size fractions were prepared for the various experiments described below: 100–200 μm and 200–500 μm. Prepared powder was ultrasonically cleaned using alcohol to remove fine particles and dried overnight at 60 °C. The specific surface area (SSA) of the cleaned powders was 570 ± 30 and 366 ± 20 cm^2/g, respectively, as determined by Kr adsorption using the multi-point (10–15 adsorption data points) B.E.T. method (SSA_{BET}). Microscopic analysis of fresh and altered forsterite surfaces was performed using a Jeol JSM840a scanning electron microscope with graphite metallization.

All input and output solutions were analyzed for magnesium ($[Mg^{2+}]_{tot}$), silica ($[SiO_2(aq)]_{tot}$), alkalinity ([Alk]), pH and organic ligands as a function of time. Alkalinity was determined following a standard HCl titration procedure with an uncertainty of ±1% and a detection limit of 5×10^{-5} M. The concentration of organic ligands was measured as total dissolved organic carbon (DOC) using a TOC Shimadzu VSCN analyzer with an uncertainty of 5% and a detection limit of 0.1 mg C_{org} L^{-1}. Magnesium concentration was measured by flame atomic absorption spectroscopy with an uncertainty of 1% and a detection limit of 1×10^{-7} M. Total silica concentration was determined using the molybdate blue method with an uncertainty of 2% and a detection limit of 3×10^{-7} M. NIST buffers (pH = 4.008, 6.865, and 9.180 at 25 °C) were used for calibration of a combination pH-electrode (Schott Geräte H62). Precision of pH measurement was ±0.01 units. At elevated pCO_2 pressure and 25 °C, in situ pH was measured with an uncertainty of ±0.05 units using solid-contact Li, Sn glass electrode coupled with Ag/AgCl reference electrode calibrated in a series of 0.1 M NaCl solutions and operating in 0.1 M NaCl as described previously (Pokrovsky et al., 2005b, 2009a).

Homogeneous solution equilibria as well as surface speciation were calculated for each solution composition using the MINTEQA2 code and MINTEQA2 thermodynamic database (Allison et al., 1991) updated from Critical Database (Martell et al., 1997). The activity coefficients of free ions and charged complexes were calculated using the Davies equation which is standard in MINTEQA2.

2.2. Bacteria cultures

Following the sampling of natural water at the CarbFix injection site (Hellisheidi, Iceland; Gislason et al., 2010) with a sampling protocol aiming at reducing contamination risks, we separated, using cultures on nutrient agar plates, four different groups of gram-negative aerobic bacteria. The enzymatic activity of studied species has been evaluated using Biolog Ecoplates using 30 different substrates in three replicates. Their phylogenetic affiliation was performed by DNA extracting (UltraClean® Microbial DNA Isolation Kit MO BIO) and 16S rRNA gene amplifying (bacterial-specific primers 8F (5′-AGAGTTTGATCCTGGCTCAG) and prokaryote-specific reverse primers 1492R (5′-GGT TACCTTGTTACGACTT), see Gérard et al., 2009 for the condition of PCR amplification) and sequencing (Cogenics, Beckman Coulter Genomics). The sequence was then identified by BLAST against the NCBI non-redundant nucleotides database. We found that Gammaproteobacterium HK31.3 associated with the wells HK31 (see Gislason et al., 2010 for description) and *P. reactans* strain SR3 (Genbank ID GQ258636), share 100% identity over 927 bases at the level of their 16S RNA genes (GenBank accession number BankIt1496454 HK31.3 JQ071900). *Pseudomonas* strains is a common groundwater microbe frequently observed in repository environments (e.g., Nazina et al., 2006, 2010). For most experiments, cells were first cultured to a stationary stage on a shaker at 25 °C in the darkness using final 10% NB with the following composition: 0.1 g/L glucose, 1.5 g/L peptone, 0.6 g/L NaCl and 0.3 g/L yeast extract.

Dead (heat-killed) cells were produced via autoclaving 30 min at 130 °C the freshly grown bacterial biomass followed by thorough rinsing in sterile 0.1 M NaCl. Inactivated cells were produced using 0.01 M sodium azide (NaN_3) for the full duration of experiments. The use of NaN_3 as metabolic inhibitor for heterotrophic bacteria is well established (i.e., Urrutia Mera et al., 1992; Johnson et al., 2007). Another stock of dead cells was prepared via treating suspension of live bacteria in 4% glutaraldehyde solution during 4 h.

Active bacteria number count (colony forming-units, CFU mL^{-1}) was performed using Petri dishes inoculation on nutrient agar (0.1, 0.2 and 0.5 mL of sampled solution in three replicates with an uncertainty of 10–20%) in a laminar hood box. Inoculation of blanks was routinely performed to assure the absence of contamination from external environment. The biomass of live bacteria suspension was also quantified by measuring wet (centrifuged

15 min at 10,000 rpm) and freeze-dried weight in duplicates. Before the batch experiment inoculation, cells were rinsed twice in appropriate fresh culture media or sterile 0.1 M NaCl solution using centrifugation (~500 mL of solution for 1 g of wet biomass) to remove, as possible, the adsorbed metals and cell exudates from the surface. Typical live biomass concentration during batch experiment ranged from 0.5 to 8 g_{wet}/L. All adsorption and dissolution experiments described below (Sections 2.3–2.5) were conducted with freshly-grown bacterial cultures having the identical age, physiological and initial nutritional status. Every new experiment started with washed bacterial culture grown to the beginning of stationary stage using identical nutrient composition and biomass yield.

2.3. Live bacteria interaction with mineral-free solutions in the presence of Mg and Si

These experiments aimed to quantify the amount of Mg and Si that could be retained by bacteria via both long-term intracellular uptake process (active assimilation) and passive adsorption at the cell wall. They also allow assessing eventual bioprecipitation process (presence of bioinduced mineralizations on the cell walls or in the media due to metabolically induced changes of chemical conditions). Conversely, a release of both Mg and Si from bacterial biomass as a result of cell lyses may occur. Experiments were performed in duplicates with 1–8.5 g_{wet}/L rinsed biomasses of *P. reactans* HK31.3 and the initial concentrations of Si and Mg ranging from 100 to 200 and from 4 to 150 μmol/L, respectively. Three types of solutions were used: (1) a 10% NB protein-rich media amended with 0.01 M NaCl and 0.01 M $NaHCO_3$ to account on active bacterial growth and intracellular uptake in cells; (2) the same media with 0.01 M NaN_3 to prevent bacterial metabolism and assess Mg and Si interaction with bacterial cell walls without active assimilation and (3) nutrient-free 0.01 M NaCl + 0.01 M $NaHCO_3$ solution with 0.01 M NaN_3 to allow cell lysis and minimum element uptake. Polypropylene vials with biomass were shaken in the dark at 25 °C and periodical sampling consisted of measuring pH, optical density, bacterial number by agar plate counting, filtration through 0.45 μm membrane and Mg and Si analysis. No difference in Mg and Si concentration was found for filtration through 0.45 and 0.22 μm membranes suggesting that cell fragments were successfully removed. Typical duration of experiments was 220 h.

2.4. Mg adsorption on bacteria

Magnesium adsorption experiments were designed to provide quantitative characterization of metal binding by bacteria surface via passive adsorption in a wide range of pH and Mg^{2+} concentration in solution. For this purpose, two types of experiments with NaN_3-inactivated bacteria were performed: (i) adsorption at constant initial magnesium concentration in solution as a function of pH (pH-dependent adsorption edge assessment) and (ii) adsorption at constant pH as a function of magnesium concentration in solution ("Langmuirian" adsorption isotherm assessment). Altogether, we conduced four series of experiments in individual batch reactors with 20–30 independent data points in each. The final adsorption parameters are based on statistical treatment of 10–15 independent measurements for the maximal adsorption site density and 20–30 independent measurements for the stoichiometry of adsorption reaction.

All solutions were undersaturated with respect to magnesium oxide, hydroxide and carbonate phase as verified by calculation using the MINTEQA2 computer code and corresponding database (Allison et al., 1991). Adsorption experiments were conducted at 25 ± 0.5 °C during 4–24 h in continuously agitated suspension of 0.1 M NaCl + 0.01 M NaN_3 solution using 8 mL sterile polypropylene vials. Manipulations were conducted in sterile laminar hood box (A100). The biomass concentration was fixed at 20 g_{wet}/L and magnesium concentration in solution ($[Mg^{2+}]_{aq}$) spanned from 3 to 1100 μM. The pH was adjusted by adding aliquots of NaOH (0.1 and 0.01 M) or HCl (1, 0.1 and 0.01 M). Constant pH was maintained by adding 0.005 M MES (2-morpholinoethanesulfonic acid monohydrate) buffer and 0.01 M $NaHCO_3$ to yield a pH of 5.7 and 7.4, respectively.

For all experiments, sterile de-ionized water (MilliQ, 18 MΩ) purged with N_2 to remove CO_2 was used. Harvested biomass was rinsed in 0.1 M NaCl solution, 0.01 M EDTA solution for 15 min and again in 0.1 M NaCl solution prior the experiments. This allowed removal of all possible surface-adsorbed Mg^{2+}, Ca^{2+} ions originated from the culture media and significantly decreased the release of intracellular Mg that was incorporated during bacterial growth. At the end of the experiment, the suspension was centrifuged and the resulting supernatant filtered through a 0.45 μm acetate cellulose filter, acidified with ultrapure nitric acid and stored in the refrigerator until analysis. The adsorption of magnesium on cell surface was quantified by subtracting, at each solution pH, the concentration of magnesium remaining in bacterial suspension from concentration of added magnesium in the supernatant (control experiments without biomass). The adsorption of magnesium on reactor walls and cellular Mg release from the biomass in the full range of studied pH was negligible (<10%) compared to the amount of Mg added to the reactor. It was routinely verified by Mg analyses in blank (supernatant) experiments and in cell suspension without added Mg and explicitly taken into account to calculate the adsorption yield.

The reversibility of Mg adsorption was tested following the method developed by Fowle and Fein (2000). A homogeneous parent suspension of 20 g_{wet}/L bacteria + 20 μM Mg + 0.1 M NaCl was adjusted to pH ~ 8.5–9, at which ~90% Mg was adsorbed onto microbial cells. After 20 h of adsorption contact time, aliquots of this parent suspension solution were taken and adjusted to sequentially lower pH values (2–8). The reaction vessels equilibrated at new pH values for 20 h were sampled for Mg. The concentration of "desorbed" magnesium in the supernatant allowed calculation of the amount of irreversibly "incorporated" metal. This amount never exceeded 5–10% suggesting an equilibrium adsorption process with negligible amount of magnesium penetrating inside the cell at the conditions of our

experiment. The second test for reversibility, used earlier for algae and bacteria (Slaveykova and Wilkinson, 2002; Smiejan et al., 2003) consisted of treating the cell suspension with 0.01 M EDTA solution for 10 min at neutral pH, and separating the cells and the supernatant by centrifugation and filtration. The dissolved (<0.22 μm) magnesium concentration were measured in the filtrate. In both cases, very good recovery (>95%) of adsorbed Mg was achieved suggesting a truly reversible adsorption process.

2.5. Olivine dissolution experiments

The summary of olivine dissolution experiments with *P. reactans* is presented in Tables 1 and 2. Altogether, 10 high pCO_2 long-term multi-point batch experiments (two of them in duplicates), six ambient conditions batch experiments (all in duplicates) (Table 1) and 32 bacterial mixed-flow experiments (4–5 replicates for each steady-state rate measurements) were performed (Table 2).

Table 1
Results of batch experiments. Olivine powder of 100–200 μm, SSA BET (Initial) = 570 ± 30 cm^2/g.

Exp. No.	Mass, g/L	Bacteria	Biomass, g_{wet}/L	Final BET, cm^2/g	Range of CFU/mL, initial–final	Media
Batch Ti high-pressure reactor with in situ pH measurements; 0.1 M NaCl, 0.05 M $NaHCO_3$, pCO_2 = 30 atm:						
1	0	Live	0.28	N.D.	4.8×10^6–3.8×10^3	10% nutrient (NB)
2	1.5	Live	1.6	352 ± 20	2.8×10^6–3.6×10^3	10% nutrient (NB)
4	1.72	Autoclaved	1.5	473 ± 30	<1–10	10% nutrient (NB)
5	1.4	Live	3.0	554 ± 35	3×10^6–10	Nutrient-free
6	0.72	Autoclaved	3.1	N.D.	500–5	Nutrient-free
7	0.80	Treated in glutaraldehyde	4.4	N.D.	100–10	Nutrient-free
10	1.56	Live	6.6	N.D.	1×10^8–2×10^6	10% nutrient (NB)
11	1.66	Inactivated in NaN_3	6.6	N.D.	2.5×10^6–10	10% nutrient (NB)
12[a]	1.37	Absent	0	N.D.	<1	10% nutrient (NB)
13[a]	1.39	Absent	0	N.D.	<1	Nutrient-free
Batch reactors without dialysis membrane:						
L1[a]	0.906	Live, no aeration	1.0	N.D.	3×10^8–4×10^6	10% NB, 0.1 M NaCl, 0.05 M $NaHCO_3$
L2[a]	0.986	Live, aeration	1.0	N.D.	3.6×10^8–1.5×10^6	10% NB, 0.1 M NaCl, 0.05 M $NaHCO_3$
L3[a]	0.818	Live, no aeration	1.0	N.D.	1.8×10^8–3.8×10^6	10% NB, 0.1 M NaCl, 0.05 M $NaHCO_3$
L4[a]	0.954	Live, aeration	1.0	N.D.	4.0×10^8–3.2×10^6	10% NB, 0.1 M NaCl, 0.05 M $NaHCO_3$
Batch reactors with 6–8 kDa dialysis membrane:						
L7[a]	0.834	Live, aeration	1.2	N.D.	$3.2 \times 10^8 \times 3.6 \times 10^6$	10% NB, 0.1 M NaCl, 0.05 M $NaHCO_3$
L9[a]	0.918	Live, aeration	0.9	N.D.	2.8×10^8–3.2×10^7	10% NB, 0.1 M NaCl, 0.05 M $NaHCO_3$

Experiment, Ng	Duration, h	pH (range)	Log R_{Si}	Log R_{Mg}	Log $R_{average}$
1	1192	4.65 ± 0.05	N.D.	N.D.	N.D.
2	1182	4.45 ± 0.05	−12.42 ± 0.02	−12.34 ± 0.03	−12.38 ± 0.04
4	407	4.35 ± 0.05	−12.45 ± 0.02	−12.51 ± 0.03	−12.48 ± 0.03
5	290	4.60 ± 0.03	−12.42 ± 0.03	−12.63 ± 0.02	−12.53 ± 0.10
6	688	5.05 + 0.05	−12.48 ± 0.01	−12.48 ± 0.01	−12.48 ± 0.01
7	688	4.67 + 0.03	−12.39 ± 0.02	−12.44 ± 0.03	−12.41 ± 0.03
10	1589	4.35 ± 0.10	−12.58 ± 0.02	−12.67 ± 0.02	−12.63 ± 0.04
11	1589	4.25 ± 0.05	−12.56 ± 0.02	−12.59 ± 0.03	−12.58 ± 0.02
12[a]	1029	5.08 ± 0.05	−12.49 ± 0.05	−12.27 ± 0.06	−12.38 ± 0.10
13[a]	1029	4.57 ± 0.07	−12.36 ± 0.03	−12.33 ± 0.05	−12.35 ± 0.03
L1[a]	1720	7.8 ± 0.1	−13.94 ± 0.02	−13.88 ± 0.02	−13.91 ± 0.03
L2[a]	1720	7.5 ± 0.2	−13.74 ± 0.02	−13.70 ± 0.02	−13.72 ± 0.02
L3[a]	1720	7.4 ± 0.1	−13.84 ± 0.02	−13.80 ± 0.02	−13.82 ± 0.02
L4[a]	1720	6.7 ± 0.1	−13.98 ± 0.06	−13.69 ± 0.05	−13.84 ± 0.14
L7[a]	1786	7.4 ± 0.15	−13.75 ± 0.08	−14.01 ± 0.04	−13.88 ± 0.13
L9[a]	1786	6.7 ± 0.1	−13.66 ± 0.02	−13.61 ± 0.02	−13.64 ± 0.02

[a] Experiments conducted in duplicates. N.D. stands for non determined.

Table 2
Results of mixed-flow experiments. Solution composition: 0.1 M NaCl + 0.01 M $NaHCO_3$ at pH 9, 0.1 M NaCl + 0.01 M MES at pH 6. Olivine powder of 200 to 500 μm size fraction with SSA BET (Initial) = 366 ± 20 cm^2/g was used in all experiments.

N	Powder, g	SSA_{final}, cm^2/g	Time, days	Debit, mL/min	Inlet solution	CFU, ml/L	DOC, mg/L	Mg, μM	Si, μM	pH	Rates, $mol/cm^2/s$		
											Log R_{Mg}[a]	Log R_{Si}[a]	Log $R_{average}$
08-1	1.047		7	0.0258	10^{-6} M gluconate	<1	0.2	5.12	2.10	6.85	−14.50	−14.63	−14.56 ± 0.06
08-2			14	0.0236	10^{-4} M gluconate	<1	20	5.39	2.07	6.28	−14.52	−14.67	−14.60 ± 0.08
08-3			21	0.0243	0.001 M gluconate	<1	190	3.37	2.10	6.20	−14.71	−14.65	−14.68 ± 0.03
08-4		372 ± 20	31	0.0251	0.01 M gluconate	<1	1900	73.3	35.3	6.29	−13.36	−13.41	−13.39 ± 0.03
06-1	0.984		6	0.0446	10^{-6} M Gluconate	<1	0.2	1.48	1.21	9.06	−14.77	−14.60	−14.69 ± 0.09
06-2			11	0.0423	10^{-4} M gluconate	<1	20	1.01	1.31	9.03	−14.96	−14.59	−14.78 ± 0.19
06-3			18	0.0419	0.001 M gluconate	<1	190	1.02	0.634	8.90	−14.97	−14.91	−14.94 ± 0.03
06-4		301 ± 15	32	0.0415	0.01 M gluconate	<1	1900	1.23	0.677	8.92	−14.88	−14.89	−14.89 ± 0.03
07-1	1.13		7	0.04	No bacteria	<1	0.8	2.06	3.24	6.05	−14.74	−14.28	−14.51 ± 0.23
07-2			11	0.0455	1.24 g_{wet}/L dead	<1	9	3.99	3.88	6.08	−14.40	−14.15	−14.27 ± 0.12
07-3			18	0.042	2.34 g_{wet} /L dead	<10	13	12.9	4.77	6.10	−13.92	−14.09	−14.01 ± 0.09
07-4			32	0.043	7.70 g_{wet} /L dead	<10	22	12.5	7.41	6.12	−13.93	−13.89	−13.91 ± 0.03
05-1	1.073		7	0.0394	No bacteria	<1	0.6	2.06	3.56	9.06	−14.72	−14.23	−14.47 ± 0.25
05-2			11	0.0375	1.24 g_{wet}/L dead	<1	4	1.32	2.07	9.02	−14.94	−14.48	−14.71 ± 0.23
05-3			18	0.036	3.36 g_{wet}/L dead	<10	9	3.05	2.31	8.95	−14.59	−14.45	−14.52 ± 0.07
05-4			32	0.036	7.0 g_{wet}/L dead	<10	13	1.69	1.67	8.90	−14.85	−14.59	−14.72 ± 0.13
01-1	0.600		7	0.049	No bacteria, no nutrients	<1	N.D.	2.88	2.10	8.90	−14.23	−14.11	−14.17 ± 0.06
01-2			14	0.047	1.2 g_{wet}/L live, 10% NB	(1.45 ± 0.15) × 10^8	N.D.	3.09	5.34	8.10	−14.22	−13.72	−13.97 ± 0.25
01-3			18	0.0459	5.3 g_{wet}/L live, 18% NB	(8.0 ± 2.0) × 10^8	N.D.	2.80	3.42	8.00	−14.27	−13.92	−14.10 ± 0.17
01-4		366 ± 20	48	0.0425	No bacteria, 0.01 M NaN_3	<1	0.5	2.06	2.81	8.91	−14.44	−14.04	−14.24 ± 0.20
02-1	0.640		7	0.0466	No bacteria, no nutrients	<1	3.7	4.12	3.67	8.90	−14.12	−13.91	−14.02 ± 0.11
02-2			14	0.0454	1.2 g_{wet}/L live, no nutrients	(1.0 ± 0.2) × 10^8	6.9 ± 1.0	4.12	2.73	8.67	−14.14	−14.05	−14.09 ± 0.04
02-3			18	0.0429	5.3 g_{wet}/L live, no nutrients	(9.0 ± 1.0) × 10^8	24.5 ± 0.5	2.51	3.53	8.10	−14.38	−13.97	−14.17 ± 0.20
02-4		352 ± 20	48	0.042	No bacteria, 0.01 M NaN_3	<1	1.0	1.98	2.28	8.90	−14.49	−14.17	−14.33 ± 0.16
03-1	0.839		7	0.027	No bacteria, no nutrients	0	0.5	22.6	18.9	6.50	−13.74	−13.56	−13.65 ± 0.09
03-2			14	0.0252	1.2 g_{wet}/L live, 10% NB	(1.3 ± 0.3) × 10^8	N.D.	18.7	8.37	7.40	−13.85	−13.94	−13.90 ± 0.04
03-3			18	0.0248	7.72 g_{wet}/L live, 20% NB	(9.0 ± 1.0) × 10^8	N.D.	19.8	21.4	7.30	−13.84	−13.54	−13.69 ± 0.15
03-4			48	0.0372	No bacteria, 0.01 M NaN_3	<1	1.0	2.88	3.92	8.90	−14.50	−14.10	−14.30 ± 0.20
04-1	0.75		7	0.046	No bacteria, no nutrients	<1	0.1	9.55	5.27	5.58	−13.83	−13.83	−13.83 ± 0.02
04-2			14	0.0452	1.2 g_{wet}/L live, no nutrients	(4.0 ± 1.0) × 10^8	5.5	28.8	19.5	5.61	−13.36	−13.27	−13.32 ± 0.05
04-3			18	0.0451	5.3 g_{wet}/L live, no nutrients	(3.2 ± 0.8) × 10^8	13	45.3	33.8	5.80	−13.17	−13.03	−13.10 ± 0.07
04-4		524 ± 30	48	0.0418	No bacteria, 0.01 M NaN_3	<1	0.5	7.00	5.70	5.94	−14.01	−13.84	−13.93 ± 0.09

[a] Uncertainty of rate measurement is ±0.02 log *R* units.

2.5.1. Batch dissolution experiments with bacteria at 30 atm pCO_2

The aim of these experiments was to compare, under the same solution conditions, the Mg and Si release rate from 0.5–1.0 g sterilized forsterite powder of 100–200 μm size fraction in contact with dead and live bacterial cultures both in nutrient-rich (10% NB) and nutrient-free solutions. Dissolution experiments were performed in constant-pH (4.5–5.5), bicarbonate-buffered (0.05 M $NaHCO_3$), 0.1 M NaCl solutions at 30 atm of CO_2 and various concentrations of freshly-grown *P. reactans*. Sterilized Ti high-pressure reactors, stirred with a magnet-driven Parr stirrer were used.

Periodic sampling of homogeneous mineral + bacteria suspension was performed using Ti valve; all sampled solutions were immediately filtered through 0.45 μm filter, acidified and stored in the refrigerator before the analysis. Live cell concentration was routinely monitored using agar plate culturing and colony counting in three replicates with the uncertainty of 10–20%; the total biomass concentration was also followed via optical density measurement at 600 nm in two replicates with the uncertainty of 5%. Duration of experiments varied from 20 to 60 days without renewing the solution, with each experiment comprising between 12 and 20 sampling points. The final rate value was calculated from the slope of linear regression [Mg, Si] versus time including all 12–20 replicate data points. Taking into account that (1) all solutions are strongly undersaturated with respect to olivine, all other possible Mg silicates and amorphous silica and (2) there is no effect of aqueous Mg and Si concentration on forsterite forward dissolution rates in neutral solution (Schott et al., 2009), one can quantify the far-from equilibrium dissolution rates for each individual experiment using the equation:

$$R = (\mathrm{d}[\mathrm{Mg, Si}]_{\mathrm{tot}}/\mathrm{d}t)/s \quad (1)$$

where t (s) designates the elapsed time, $[\mathrm{Mg, Si}]_{\mathrm{tot}}$ (mol/L) stands for the concentration of calcium and silica released from the solid, and s (cm^2/L) is the powder B.E.T. surface area. The standard deviation 2σ (95% confidence interval) was calculated based on the ensemble of 12–20 data points in each individual experiment; the typical uncertainty did not exceed 10%. Finally, two bacteria-free experiments were performed in duplicates; the agreement between the final rate values inferred from two independent experiments was better than 20%.

2.5.2. Batch dissolution experiments with bacteria at ambient conditions

The batch reactors used to study olivine–bacteria interaction consisted of sterile 500 mL polypropylene culture flasks with vented caps (Biosilico®). Experiments were conducted in duplicates with 10–15 individual data points used to calculate the forward Mg- and Si- release rates in each independent experiment. For all experiments, 0.4–0.5 g of 100–200 μm olivine powder sterilized at 120 °C during 30 min were placed in 500 mL with 10% NB or 0.1 M NaCl solution producing a solid concentration of ~1 g/L. The reactors were inoculated with 1–2 mL of fresh *P. reactans* HK31.3 cultures or the fixed amount of dead biomass and placed on a shaker at 25 ± 1 °C. Duration of experiments ranged from 1 to 4 weeks. Sterile controls were routinely run both for nutrient media and 0.1 M NaCl + 0.05 M $NaHCO_3$ solutions and did not demonstrate any bacterial contamination. Periodically, 10 mL aliquots of homogeneous mineral suspension + bacteria were collected using sterile serological pipettes for Mg, Si, pH and cell biomass measurements. The solid/fluid ratio remained constant during experiments and the concentration of bacteria was not affected by the sampling. Mg and Si concentrations were measured in acidified 0.22 μm filtrates and pH and cell biomass were measured in unfiltered non-acidified samples. Live cell concentration was routinely monitored using agar plate culturing and colony counting; the total biomass concentration was also followed via optical density measurement at 600 nm.

2.5.3. Batch experiments with dialysis membrane

In order to distinguish the direct effect of bacterial cells and indirect effect of bacterial exudates on mineral dissolution, experiments were designed such that the mineral powder was separated from bacterial suspension using a dialysis membrane of 6–8 kDa (~2–3 nm) cutoff. These experiments were conducted in duplicates with 7–12 individual data points used to calculate the forward Mg- and Si-release rates. For this, 500-mL sterile flasks were fitted with 0.5 g of 100–200 μm sterilized olivine powder enclosed in dialysis compartment which was submerged in bacterial suspension of live or dead cells, in 0.1 M NaCl containing 0.05 M $NaHCO_3$ or 0.01 M NaMES buffer with or without nutrient (as 10% NB). Periodically, 5 mL of external solution were sampled under sterile environment and analyzed for total biomass, number of active cells, pH, Mg and Si concentrations. The dissolution rate R_{average} was calculated from the slope of [Mg], [Si] – elapsed time dependence and averaged from R_{Mg} and R_{Si} values taking into account the slight increase (ca. max. 10%) of the mineral/solution ratio during the course of experiment due to sampling of external solution.

2.5.4. Mixed-flow dissolution experiments

New design of Bacterial Mixed-Flow Reactor (BMFR) system was used in this study. These reactors allow computing steady-state dissolution rate based on several (at least five) replicates of independent measurements. Typically, two parallel reactors were employed for rate quantification at each solution composition and bacterial concentration. The experiments were aimed at assessing the dissolution rate variation as a function of concentration of live and dead bacteria at two different pHs (6 and 9).

Steady-state dissolution rates were obtained at distinct solution compositions and pH using a mixed-flow reaction vessel immersed in a water bath held at a constant temperature of 25.0 ± 0.5 °C. Prior the experiment, all reactor system including tubing was sterilized at 130 °C during 30 min and rinsed by sterile MilliQ water. The cultures for each single experiment were harvested at the end of exponential stage and prepared using exactly the same experimental protocol (see Section 2.2). The input fluid containing live or dead bacterial suspension in 0.1 M NaCl with or without

10% NB was kept in 1-L polypropylene bottles closed with Biosilico ventilated caps under continuous stirring during the experiments and was changed typically each 7 days. This allowed maintaining the constant and stable stationary phase of bacterial culture in the inlet fluid as proven by live bacteria count, optical density measurement and monitoring the DOC concentration. Bacterial suspension was injected into the reaction vessel using pre-sterilized Gilson® peristaltic pump using 2-mm inner diameter silicon tubing and typical flow rate ranging from 0.02 to 0.05 mL/min. The reactor consisted of completely filled 50-mL Teflon® beaker which was continuously stirred with a floating Teflon supported magnetic stirrer. Stirring was controlled by a stirplate located directly beneath the bath. The reactive solution left the reactor through a 20 μm pore size nylon filter that allowed the passage of bacterial cells but retained the mineral powder (0.5–1.0 g of 200–500 μm olivine grain having SSA_{BET} of 366 cm^2/g). The outlet solutions were additionally filtered through a 0.45 μm acetate filter. No differences in analytical Mg and Si concentrations were detected compared to 20 μm nylon filtered samples suggesting that the adsorption of reaction products on bacterial cells or lysis products was negligible. The inlet and outlet fluids were periodically sampled for cell optical density (total biomass) and number of live cells (agar plate counting). This also allowed monitoring possible contamination of the system by other culturable heterotrophic bacteria based on microscopic agar plate colonies examination.

Reacting fluids were comprised of deionized degassed H_2O, Merck reagent grade 0.1 M NaCl, 0.01 M $NaHCO_3$ or 0.01 M NaMES buffer. Experiments with dead bacteria were always performed in the presence of 0.01 M NaN_3 to prevent external bacterial contamination. Two experiments were performed in bacteria-free system in the presence of gluconic acid, a typical exometabolite of heterotrophic bacteria (e.g., Welch and Vandevivere, 1994; Welch and Ullman, 1999). Solution compositions in this set of experiments are listed in Table 2.

Mechanical steady-state in reactor was achieved after 24 h of reaction. Each experiment involved new olivine powder which was reacted with consequently increasing bacterial or ligand concentrations. For each steady-state condition, 4–5 measurements of Mg and Si concentration, pH and flow rate was recorded (reproducibility of ±10%) and used for calculating the average dissolution rate. We used a criterion of average Mg and Si concentration at steady state as ±5% at $[Mg^{2+}]_{tot} \geqslant 5\ \mu M$ and ±15% at $[Mg^{2+}]_{tot} < 5\ \mu M$, measured after achieving three times mechanical steady state. Due to the possibility of Mg, Si release from bacterial biomass in the inlet reservoir, we periodically sampled the inlet suspension before the reactor, filtered and analyzed for Si and Mg concentrations. These values never exceeded 30% of the outlet concentrations and therefore; necessary corrections for rate calculations were made.

Steady-state dissolution rates (R_i, mol/cm^2/s) given in Table 2 were computed from measured solution composition using

$$R_{Si} = -q \cdot \Delta[SiO_2(aq)]_{tot}/s$$

and

$$R_{Mg} = -q \cdot 0.55 \cdot \Delta[Mg^{2+}]_{tot}/s$$

where q (L/s) designates the fluid flow rate, $\Delta[SiO_2(aq)]_{tot}$ and $\Delta[Mg^{2+}]_{tot}$ (mol/L) stands for the difference between the input and output silica and magnesium solution concentration, respectively, s (cm^2) refers to the total mineral surface area and coefficient 0.55 corresponds to Mg:Si molar ratio in the solid phase. The surface area used to calculate the rates listed in Tables 1 and 2 were that measured on the fresh (unreacted) forsterite powder.

In order to account for possible adsorption of aqueous Mg by the biomass surface, that would lead to underestimation of the rate, outlet suspension was periodically collected and treated during 10 min with 0.01 M EDTA using centrifugation. The amount of Mg released in solution after EDTA treatment was considered as reversibly adsorbed on the surface (e.g., Knauer et al., 1997; Le Faucher et al., 2005). This amount never exceeded 10% of total dissolved (<0.45 μm) filtered concentration and therefore was not considered in the mass balance of mineral dissolution in the presence of bacteria.

2.6. Statistics

Rates and element concentration data were analyzed by linear regression, Pearson correlation and one-way ANOVA with STATISTICA software package (Release 7, Stat Soft. Inc., USA). Regressions and correlation coefficients were used to examine the relationships between element concentration and time in batch reactors. ANOVA was used to test the differences in average element concentrations and bacterial biomass among experiments with different nutrient conditions and pH. Normal probability plots of residuals from regressions were used to test the assumptions of normality.

3. RESULTS

3.1. Bacterial culture characteristics

The optimal growth conditions of the bacterium *P. reactans* on Nutrient Broth Fluka 25 g/L (NB) have been determined as 5 to 37 °C and pH of 7.5–8.2 (not shown). Growth on protein-free, glucose- and phosphate-bearing media was almost negligible, in accord with results of the Biolog Ecoplates analyses. Bacterial growth was inhibited by the presence of 0.02–0.05 M Na_2CO_3 but in general it was weakly sensitive to the presence of bicarbonate and carbonate ions in a wide range of pH, from circumneutral to alkaline. Results are illustrated in Fig 1 which presents the biomass yield as a function of time based on two replicates. In these experiments, the pH evolution was similar (within ±0.3 units) among the experiments with different concentration of $NaHCO_3$ (from initial 9.0 to final 7.5) and that of Na_2CO_3 (from the initial 10.5 to the final 7.5). It follows from this figure that, in the range of $NaHCO_3$ and Na_2CO_3 concentrations used in our study to measure olivine dissolution rates (0–0.05 M $NaHCO_3$; 0–0.01 M $NaHCO_3 + Na_2CO_3$, see

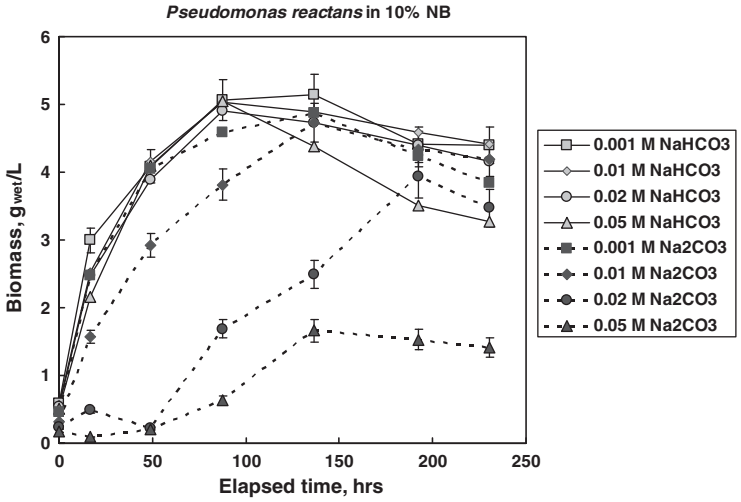

Fig. 1. Growth of *P. reactans* in 10% nutrient media (NB) in the presence of different concentrations of $NaHCO_3$ and Na_2CO_3 solutions. The evolution of pH value was similar among the experiment in the presence of different concentration $NaHCO_3$ (from initial 9.0 to final 7.5) and Na_2CO_3 (from initial 10.5 to final 7.5). Symbols correspond to results of duplicate measurements with 2σ uncertainty and the lines connecting the data points are for the aid of the reader.

Section 2.5), cell growth does not depend on $[NaHCO_3]$ and $[Na_2CO_3]$.

The conversion factor wet/freeze-dried weight for studied microorganisms determined in three replicates was found to be equal to 8.4 ± 0.5. The conversion factor of optical density (600 nm, 10 mm path) and wet biomass (g/L) to the cell number (CFU/mL) was equal to $(5 \pm 1) \times 10^8$ and $(8.0 \pm 1.5) \times 10^7$, respectively as determined by analyses of five replicates.

3.2. Mg adsorption

The pH-dependence of Mg adsorption on bacteria surfaces demonstrates the following general features as shown in Fig. 2A. After 4 h of exposure, at pH below 4, there is no or little adsorption. The adsorption edge occurs at pH from 4 to 7 and above pH 8, the maximum of adsorption is observed. With further pH increase from 10 to 12, there is a pronounced decrease in adsorption, probably linked to cell lysis and surface layer degradation. The concentration of adsorbed Mg as a function of equilibrium Mg concentration in solution ($[Mg^{2+}]_{aq}$) at pH of 5.7 and 7.4 after 24 h of exposure for live inactivated *P. reactans* is shown in Figs. 2B. Three features of adsorption phenomena should be noted. The slopes of dependences between adsorbed and aqueous Mg remain constant over two orders of magnitude of $[Mg^{2+}]_{aq}$, suggesting a similar surface adsorption mechanisms controlling Mg distribution in the system. At the same time, while this slope is equal to 1 at pH of 5.7, it is close to 0.5 for experiment at pH = 7.4 (Fig. 2B). This may be linked to a single surface adsorption reaction at pH 5.7 (for example, carboxylate groups) and multiple surface moieties participating in Mg adsorption at pH 7.4 (carboxylate, phosphate, hydroxylate). Finally, the maximal surface adsorption density (surface site saturation) is attained at $[Mg^{2+}]_{aq} \geqslant 800$–$1000\ \mu M$ and equals to 7–8 μmol Mg/g_{wet} at both pH (Fig. 2B). For typical concentration of bacteria in kinetic experiments of 2–4 g_{wet}/L, it means that 14–32 μmol/L of Mg can be complexed with bacterial surface via reversible adsorption.

3.3. Biomass interaction with Mg- and Si-bearing, mineral-free solution: Mg and Si uptake by cells

Concentrations of aqueous Mg and Si are plotted as a function of reaction time in duplicate experiments with live and inactivated bacteria and in nutrient-free media in Fig. 3A and B. In the range of low initial Mg concentration (4–12 μM) in nutrient-rich media during cell growth up to concentration of 1.2 $g_{wet}\ L^{-1}$, there is $\leqslant$10% decrease of [Mg], most likely linked to intracellular uptake of this element. Note however that this effect is almost within the experimental reproducibility. Extrapolating these results to typical concentration of bacteria in kinetic experiments yields that $\leqslant 1\ \mu mol\ L^{-1}$ of Mg released in solution can be consumed by bacterial cells via intracellular uptake. The Si concentration evolution during bacterial growth does not subject to any systematic variation (Fig. 3B) thus confirming that Si uptake/adsorption and release due to cell lysis are negligible at the investigated conditions.

3.4. Olivine dissolution kinetics

3.4.1. Batch experiments at 30 atm pCO_2 and pH = 4.5–5.0

SEM examination of the grain surfaces reacted in inorganic solutions and in bacteria-free nutrient media showed that they are similar to those of the fresh powder (Fig. 4A). For nutrient-free solution at pH = 4.6 (Exp. No. 13), formation of etch pits can be clearly detected (Fig. 4B). For grains reacted in nutrient media, negligible alteration of the surface has been observed (Fig. 4C), thus confirming the absence of any secondary precipitation. This is in agreement with SEM analyses of Wogelius and Walther (1991) who did not detect the precipitation of any secondary

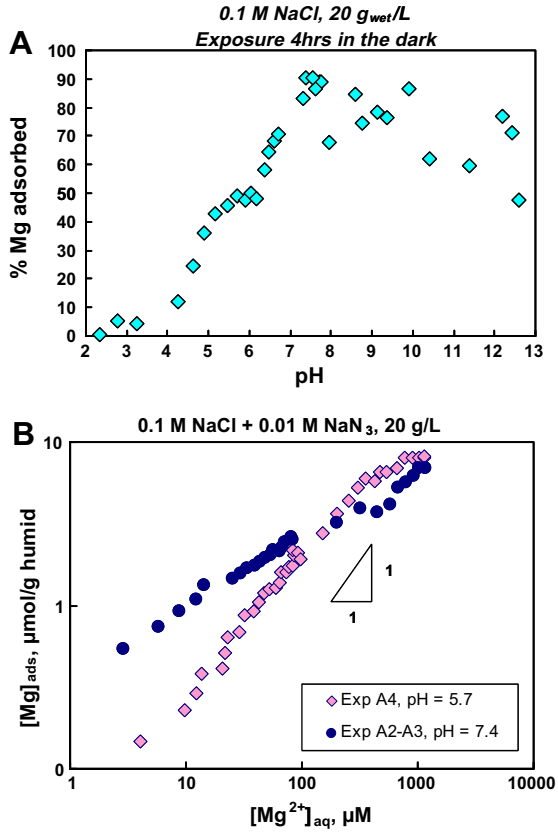

Fig. 2. Results of Mg adsorption on bacterial surface in 0.1 M NaCl + 0.01 M NaN_3 at 20 g_{wet}/L biomass concentration. (A): Percentage of adsorbed Mg as a function of pH for *P. reactans* (pH-dependent adsorption edge at $[Mg]_o = 20$ µM) (B): Concentration of adsorbed Mg as a function of Mg concentration in solution (Langmuirian adsorption isotherms) at pH = 5.7 and 7.4. Analytical error bars are within the symbol size.

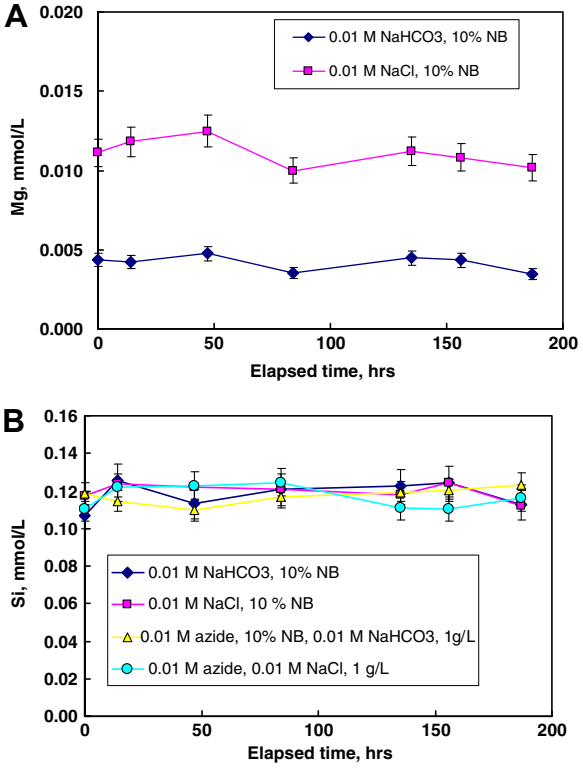

Fig. 3. Total dissolved Mg (A) and Si (B) concentration evolution as a function of time in mineral-free experiments with live (10% NB) and inactivated (0.01 M azide) bacteria. Symbols correspond to results of duplicate measurements with 2σ uncertainty and the lines connecting the data points are for the aid of the reader.

silicate minerals even in solutions about a hundred times supersaturated with respect to talc and/or chrysotile.

In contrast to bacteria-free experiments, SEM observation of grains reacted in the presence of live cells revealed the presence of biofilm-like surface coverage composed of both cells and cell exometabolites and exopolymeric substances (EPS) that may prevent mineral dissolution during long-term exposures (Fig. 4D and F). Note the appearance of typical etch pits in some parts of the surface (Fig. 4E), also visible in abiotic experiments (Fig. 4B and C). This biofilm coverage was noted mostly in experiments with live cultures in nutrient-rich solutions and distributed on 30–50% of examined grain surfaces. For NaN_3 – inactivated cultures, the olivine surface also exhibited some biofilm coverage in the form of dead cells remnants and exometabolites (Fig. 4G) although it was present only in selected zones, not homogeneously distributed over the surface (Fig. 4I). EDS analysis of selected spots on the surface (with and without biofilm coverage) yielded identical chemical composition (Mg, O, Si, Fe) with higher amount of carbon on spots with coverage. Finally, olivine grains reacted with dead (autoclaved) cultures demonstrated the presence of well preserved cells all over the surface, without specific attachment of cells to the etch pits or edges (Fig. 4J).

The change of BET specific surface area after the experiments No 4 and 5 at pH = 4.5–5 and 30 atm pCO_2 was less than 20% for live culture without nutrients and for heat-killed cells in the presence of nutrients reacted during 300–400 h. At the same time, live culture reacted with olivine grains in nutrient-bearing solutions (10% NB) during 600 h (Exp. No. 2) yielded a ~60% decrease of SSA (Table 1). This result, however, should be interpreted with caution given that no duplicate of Exp. No. 2 was conducted. Since SSA_{BET} measurements were performed on a limited number of samples, bulk olivine dissolution rates were normalized to the initial specific surface area.

The viability of cells in closed reactor at 30 atm pCO_2 always remains rather high, with total amount of live cells decreasing during the first several days by a factor of 10 but afterwards staying constant or slightly decreasing during the full duration of dissolution experiments as illustrated in Fig. 5 presenting results of triplicate measurements of live cell number by agar plate culturing.

Long-term batch dissolution experiments at pH 4.5–5.0, 0.1 M NaCl + 0.05 M $NaHCO_3$ and 30 atm pCO_2 and nutrient-free solutions yielded rates that were only weakly affected by the presence of live bacteria up to 7 g wet biomass/L (Fig. 6) as it is seen from the similarity of slopes of Mg (Fig. 6A and C) and Si (Fig. 6B and D) concentration

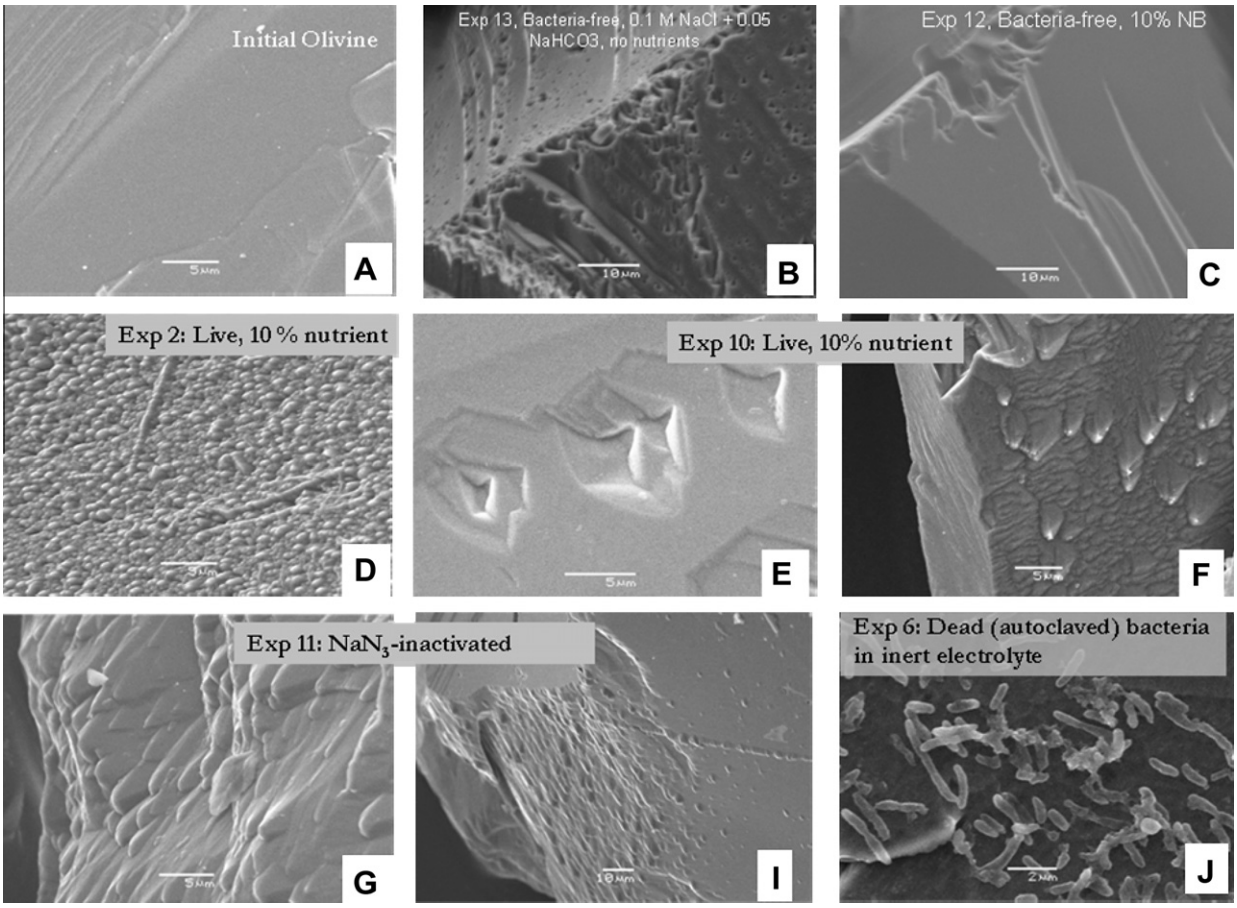

Fig. 4. SEM images of olivine surfaces reacted at 25 °C, 30 atm pCO_2, 0.1 M NaCl + 0.05 M $NaHCO_3$. (A): Initial sample; (B): olivine surface after Exp No 2 (50 days in nutrient media); (C) and (D): Etch pits and biofilm coverage after reaction during 40–50 days in nutrient-rich solution; (E): Exp. No. 11, NaN_3-inactivated; (F): Exp. No. 6 with dead (autoclaved) cells; (G): Exp. No. 13, Bacteria-free, 0.1 M NaCl + 0.05 $NaHCO_3$, no nutrients, (I): Exp. No. 12, Bacteria-free, 10% NB, and (J): Autoclaved bacteria in inert electrolyte.

dependence on time. For some experiments, there is a "plateau" of constant Mg and Si concentration attained after 150–200 h of reaction. This "plateau" is observed only in nutrient-bearing media (bacteria-free Exp. No. 12 and Exp. No. 2 with 1.6 g_{wet}/L live bacteria, Fig. 6B and D). There is no such plateau in experiments performed in inert electrolyte (No. 13), with live (Exp. No. 5), heat-killed (Exp. No. 6) and glutaraldehyde-treated (Exp. No. 7) cells in nutrient-free solutions nor for Exp. No. 10 and Exp. No. 11 (with live and NaN_3 inactivated cells, respectively) performed with nutrients. Unfortunately, without measurements of specific organic compounds, capable of inhibiting olivine dissolution, it is difficult to constrain the processes leading to the appearance of dissolution plateau in these batch reactors. Given that Exp. No. 2 demonstrated cell lysis which was more pronounced than in Exp. No. 10 (Fig. 5), it is possible that the lysis products could start to inhibit olivine dissolution after 2 weeks of reaction. Another possible explanation could be that the nutrient components such as peptone or yeast extract are capable of retarding olivine dissolution after long (~150–200 h) reaction time. At high initial biomass concentration ($\geqslant$4 g_{wet}/L), most rate-inhibiting nutrients are consumed by bacteria during the first days of experiments,

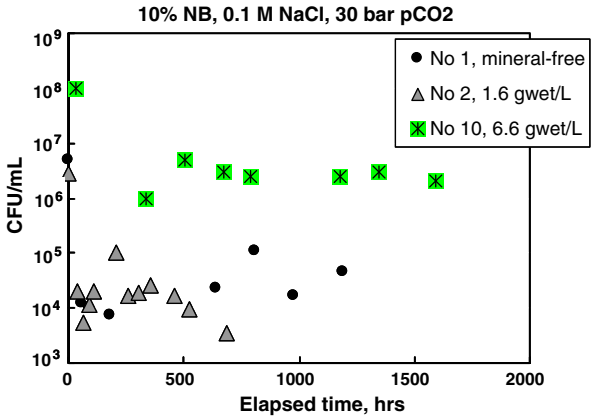

Fig. 5. Evolution of live *Pseudomonas reactans* cell concentration (CFU/mL) during the course of experiment in batch reactor at 30 atm pCO_2. The numbers represent triplicate measurements with the error bars within the symbol size.

dissolution goes forward and no inhibition at late stages occurs (Exp. No. 10). Regardless of the origin of "plateau", the bulk dissolution rates for Exp. No. 2 and 12 were computed

from the linear region of [Mg, Si] vs. time dependence, at the initial stage of dissolution where the inhibition does not occur. Except for experiments No. 2 and 12, the slopes of Mg, Si – time dependences remain essentially constant over full duration of the experiments and the rates calculated from these slopes are very similar within ±0.1–0.2 log units among all types of experiments: four abiotic nutrient-free and nutrient-bearing solutions (heat-killed cells, NaN_3-inactivated cells, glutaraldehyde-treated cell), four biotic (live cultures in nutrient-free and nutrient-rich media) and two inorganic (in duplicates) as listed in Table 1. Given the intrinsic scatter in pH values at each individual experiment that ranged from 4.3 to 5.1, this similarity is remarkable. Moreover, stoichiometric rate values obtained at 30 atm pCO_2 and 25 °C are in reasonable agreement (within ±0.3–0.5 log R unit) with those measured in mixed-flow reactor (Wogelius and Walther, 1992; Pokrovsky and Schott, 2000b) as illustrated in the plot of log R dependence on pH (Fig. 7).

Few studies have considered that heterotrophic bacteria maintained and grown for long periods in the laboratory in nutrient-rich media may not be suitable for dissolution experiments, affecting the element release from the mineral in a lesser degree than freshly cultivated organisms (e.g., Hutchens et al., 2003). To address this possibility, we performed the experiments with freshly extracted bacterial culture (No. 2), with bacteria which were reactivated after keeping in the refrigerator at 10% nutrient solution during 1 year (No. 5), and with bacteria sub-cultured on nutrient agar for 1 year (No. 10). The difference between the rates was within ±0.1–0.2 log R units; however, the highest rates were, indeed, detected in Exp. No. 2 with fresh bacterial culture.

3.4.2. *Long-term dialysis experiments*

Long-term batch dialysis experiments were designed to compare element release from olivine with and without physical contact between the mineral surface and the viable bacterial cells. In these experiments the mineral surface and the bacteria were separated by semi-permeable dialysis membrane (6–8 kDa, approx. 3 nm pore size). In the presence of 10% nutrient media, the cells remained viable over the full duration of the experiment although the number of active cell decreased more rapidly in case of physical contact between mineral and bacteria (dialysis-free set-up, Fig. 8). However, for the majority of rates calculated during

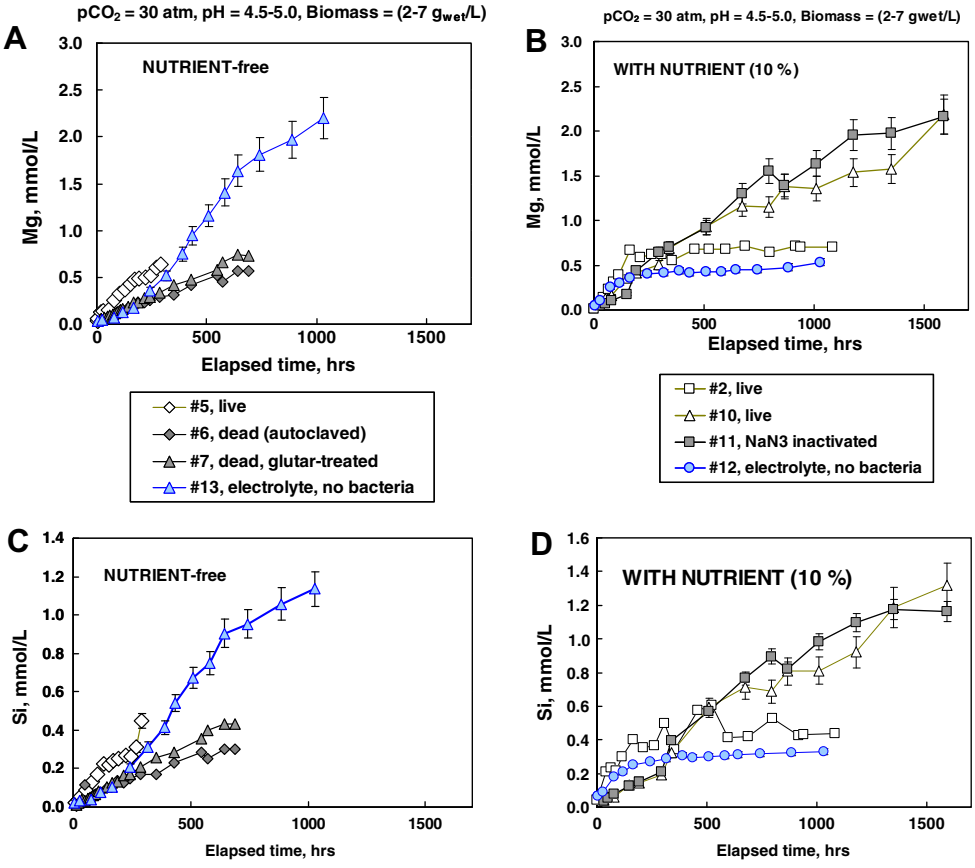

Fig. 6. Mg (A, B) and Si (C, D) concentration in solution as a function of time in batch experiments at 30 bar pCO_2 (Table 1). Long-term olivine dissolution rate at pH around 5 and 30 atm pCO_2 is only weakly affected by the presence of live bacteria up to 7 g wet biomass/L both in nutrient-free (A, C) and nutrient-rich (B, D) solutions. Open system stand for live cultures; solid (gray) symbols represent dead (inactivated) cultures and blue triangles and circles represent results of abiotic cell-free experiments. Analytical uncertainties on the data are within the symbol size unless indicated and the lines connecting the data points are for the aid of the reader. (For interpretation of the references to color in this figure legend, the reader is referred to the web version of this article.)

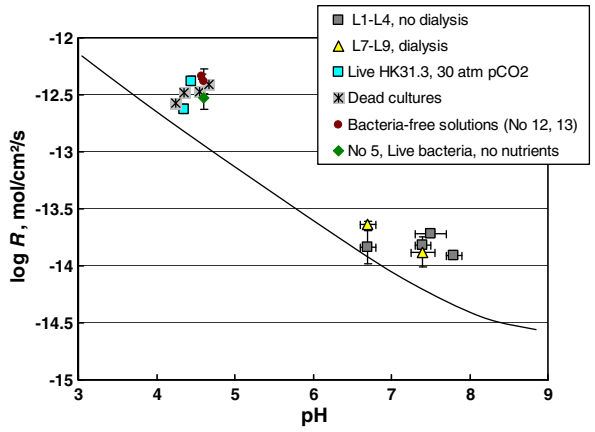

Fig. 7. Olivine dissolution rate as a function of pH measured at 25 °C in batch experiments in this study (duplicates, 5–10 sampling for each rate), at 30 atm pCO_2 (two duplicates, 15–20 sampling for each rate) and with and without dialysis compartment (all in duplicates). The error bars (2σ) are within the symbol size unless indicated. The solid line represents the data of Pokrovsky and Schott (2000b).

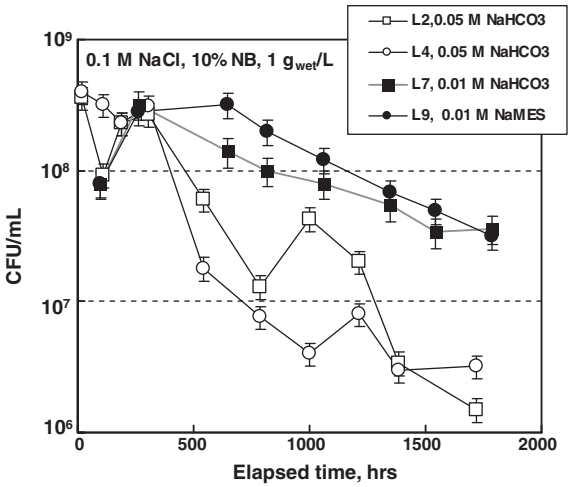

Fig. 8. Concentration of live cells as a function of elapsed time in batch experiments with and without dialysis membranes (L7-L9 and L2-L4, respectively). The numbers represent triplicate measurements with the error bars (2σ) and the lines connecting the data points are for the aid of the reader.

the first 400 h, the cell number was fairly similar for all experiments: (2–5) $\times 10^8$ cell/mL.

Over the first 400–500 h of experiment, Si and Mg release was close to stoichiometric that allowed precise rate calculation from the slope of concentration dependence on time. An example of Mg release as a function of time in dialysis experiment is given in Fig. 9. Within the experimental uncertainty ($\pm$0.2 log units), we could not reveal the difference of the dissolution rate in contact and in no-contact mode as it is illustrated in Fig. 7 where the logarithm of dissolution rate is plotted as a function of pH. The average log R values (mol/cm^2/s) for dialysis and no-dialysis experiments at pH = 6.7–7.8 are equal to -13.76 ± 0.12 and -13.79 ± 0.05, respectively.

3.4.3. Bacterial Mixed-Flow Reactor (BMFR) experiments

The steady state was typically reached after 20–50 h depending on the flow rate. For each experiment, at least five data points at steady-state conditions were collected. In most experiments performed at pH of 6–9, stoichiometric release of Si and Mg was observed. The times necessary to reach mechanical (~four fluid residence times) and chemical steady-states were very close. In alkaline solutions, the time to reach the stoichiometric steady-state dissolution at the same flow rate was much longer, up to 100 h.

For all experiments listed in Table 2, the outlet solutions were strongly undersaturated with respect to forsterite, brucite, magnesite, chrysotile and talc (saturation indices are below 0.1). Specific surface change in mixed-flow experiments was typically less than 20% with the exception of one experiment (Exp. 04, reacted 48 days at pH 6) demonstrating a 40% increase in the SSA (Table 2).

Experiments with dead bacteria (Exp. 07 and 05, Table 2) performed at pH 6 and 9, respectively, demonstrated negligible effect of biomass concentration (up to 7.7 g_{wet}/L) on Mg and Si release in alkaline solutions at pH ~ 9. In contrast, in neutral solutions at pH ~ 6, the rates increased by a factor of 2–6 with the dead biomass increase (Fig. 10). Note that the concentration of dissolved organic carbon present in the form of cell exometabolites and lysis products remained stable in a wide range of pH during the dissolution experiments at each given bacterial concentration (Table 2). The [DOC] ranged from 1 to 25 mg/L being the highest in experiments with live biomass.

Experiments with live cells yielded no systematic trend of dissolution rate with biomass at pH = 8–9 with and without nutrients in solutions containing 0.01 M $NaHCO_3$ (Fig. 11). Similar result was achieved at pH = 7.5 in carbonate-free solution, whereas at pH = 5.8 in nutrient-free system, we observed a rate increase by a factor of 5–7 with the biomass increase up to 5.7 g_{wet}/L (Fig. 12).

Finally, flow-through experiments with various concentration of gluconic acid were performed in bacteria-free systems. Gluconic acid and its derivatives are believed to be the main exometabolite of heterotrophic bacteria that use glucose as substrate (e.g., Duff et al., 1962; Welch and Ullman, 1999). Olivine forward dissolution rates measured as a function of total gluconate concentration at pH 6 and 9 are plotted in Fig. 13. It can be seen that the rates slightly decrease with gluconate concentration increase at pH = 9 and 0.01 M $NaHCO_3$ but there is a significant rate increase at pH 6 in carbonate-free solutions in the presence of >0.001 M gluconic acid.

4. DISCUSSION

4.1. Possible sinks of Mg and Si in the system

In the presence of bacteria, there are several possible sinks for mineral constituents that are being released from the forsterite surface schematically represented in Fig. 14:

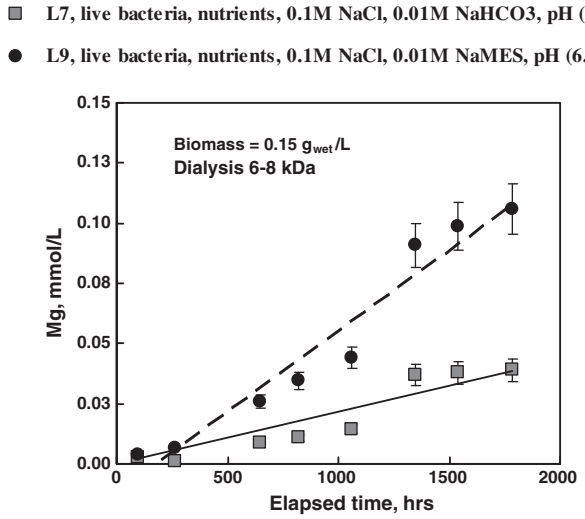

Fig. 9. Results of long-term dialysis experiments with live biomass and inert electrolyte in which the mineral surface and the bacteria were separated by semi-permeable dialysis membrane (6–8 kDa) revealed only the effect of nutrient presence on mineral dissolution. Symbols correspond to results of duplicate measurements with 2σ uncertainty (within the symbol size unless indicated) and the lines represent linear regression through the data points used to calculate dissolution rates.

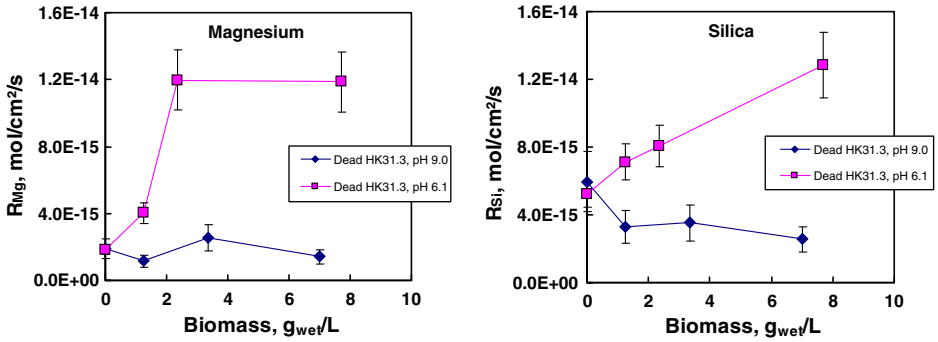

Fig. 10. Effect of dead cell concentration on Mg and Si release rate in Bacteria Mixed-Flow Reactor (BMFR), experiments 05 and 07 (Table 2). The numbers represent the average of 4–5 steady-state rate measurements with the 2σ uncertainty and the lines connecting the data points are for the aid of the reader.

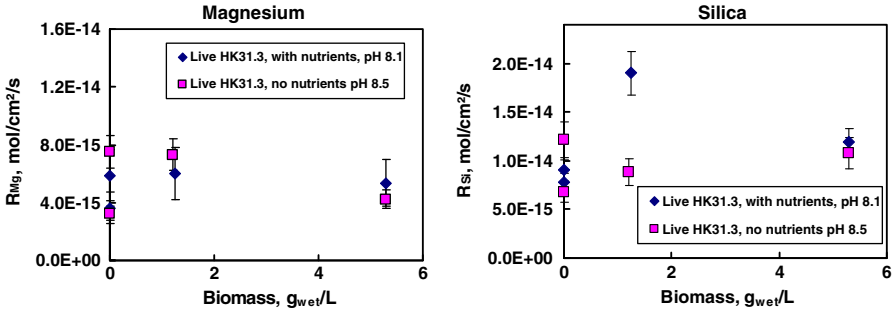

Fig. 11. Effect of live cell concentration on Mg and Si release rate in BMFR in alkaline carbonate-bearing solutions, experiments 01 and 02 (Table 2). The numbers represent the average of 4–5 steady-state rate measurements with the 2σ uncertainty.

(i) aqueous (<0.45 μm) fraction in the form of ions and molecules (Ia), simple organic complexes or organic colloids of the lysis products and cell exometabolites (Ib); (ii) fraction reversibly adsorbed at the surface of cell walls (II) and (iii) fraction irreversibly assimilated in the interior of bacteria (III). Whereas the first fraction is routinely measured after solution filtration through 0.45 μm in all dissolution experiments performed in the present study, the

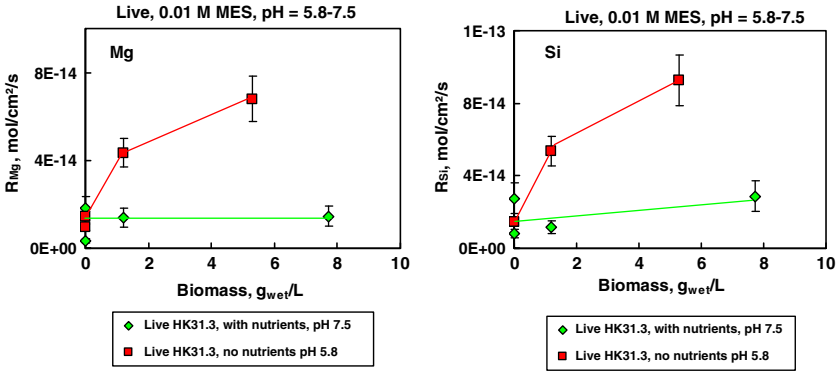

Fig. 12. Effect of live cell concentration on Mg and Si release rate in BMFR in neutral, carbonate-free solutions. The numbers represent the average of 4–5 steady-state rate measurements with the 2σ uncertainty and the lines connecting the data points are for the aid of the reader.

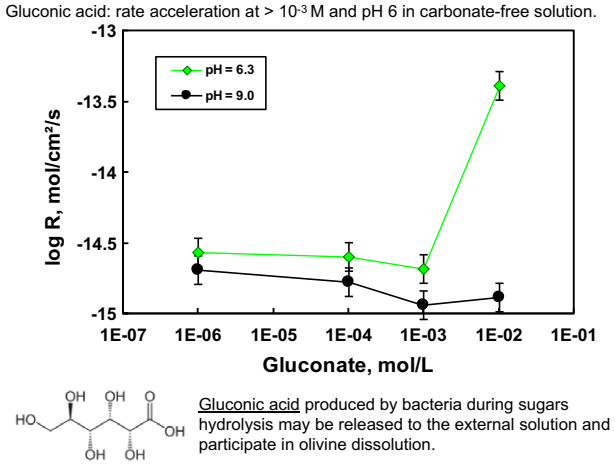

Fig. 13. Forward olivine dissolution rates in carbonate-free solutions as a function of free gluconate concentration. The numbers represent the average of 4–5 steady-state rate measurements with the 2σ uncertainty and the lines connecting the data points are for the aid of the reader.

second and the third fractions could be only estimated via bacterial growth experiments in mineral-free, Mg, Si-bearing solutions and Mg, Si desorption from the cell surface after EDTA treatment. We evaluate that the contribution of the last two fractions to the overall mass balance during olivine dissolution is less than 10–15% and as such can be neglected. Therefore, we observe a weak proportion of adsorbed or intercellular incorporated Mg and Si, despite their possible metabolic requirement. This is in contrast to trace metals that are known to be significantly uptaken by growing biomass in bacteria – mineral experiments (Neaman et al., 2005a,b, 2006).

4.2. The biofilm coverage and role of bacterial contact with mineral surface

Bacterial biofilm formation on the mineral surface is known to inhibit the dissolution (Ullman et al., 1996; Hutchens et al., 2006; Davis et al., 2007; Aouad et al., 2008; Hutchens, 2009) and the excretion of complex polysaccharides may also decrease the dissolution rate (Welch and Vandevivere, 1994; Welch et al., 1999). Besides, it was also suggested that microbially mediated dissolution of phosphates may be less effective when bacteria are in direct contact with mineral surfaces (Hutchens et al., 2006). Another example is a typical environmental bacterium, *Shewanella oneidensis* MR-1 which was reported to decrease calcite dissolution via inhibiting the formation of etch pits at screw or point dislocations due to biofilm formation on the surface (Lüttge and Conrad, 2004).

In acidic-CO_2 bearing solutions in nutrient-rich media, a biofilm-like surface coverage of reacted grains was observed. This biofilm is likely to be formed via concerted extraction of EPS material by many bacterial cells, attached together on the mineral surface. Nevertheless, the presence of such a biofilm does not appreciably affect the rate of Mg and Si release from the olivine surface. From the microscopic SEM examination of reacted grains and qualitative chemical analysis of selected spots by the EDS, we have not evidenced any secondary mineral formation within these EPS-covered surface layers. Since formation of such a biofilm occurs only in nutrient-bearing solutions, we do not expect it to be important in natural settings whose chemical composition is close to that of inert electrolyte experiments with very low [DOC]. The weak effect of bacterial coverage on olivine reactivity in acidic solutions at high CO_2 pressure is consistent with results of batch dialysis experiments at pH $\sim$ 7 and ambient conditions. The rates measured at pH = 7–8 under conditions of bacteria being in contact and non-contact with mineral grains were identical within 2σ experimental uncertainty.

4.3. Mechanisms of dissolution

The weak or slightly inhibiting effect of bacteria and their exometabolites on olivine dissolution in slightly acidic and alkaline solutions and pronounced impact of bacteria and organic compounds on olivine dissolution in neutral solutions can be understood from the knowledge of olivine surface chemistry and rate-controlling mechanisms (Pokrovsky and Schott, 2000a,b; Oelkers et al., 2009). The outermost {0 1 0} surface consists of undercoordinated Mg atoms within a loosely packed sheet of oxygens, with Si and O in the next layer down (Hochella, 1990). In acidic solutions (pH < 5), due to Mg^{2+}–H^{+} exchange reaction

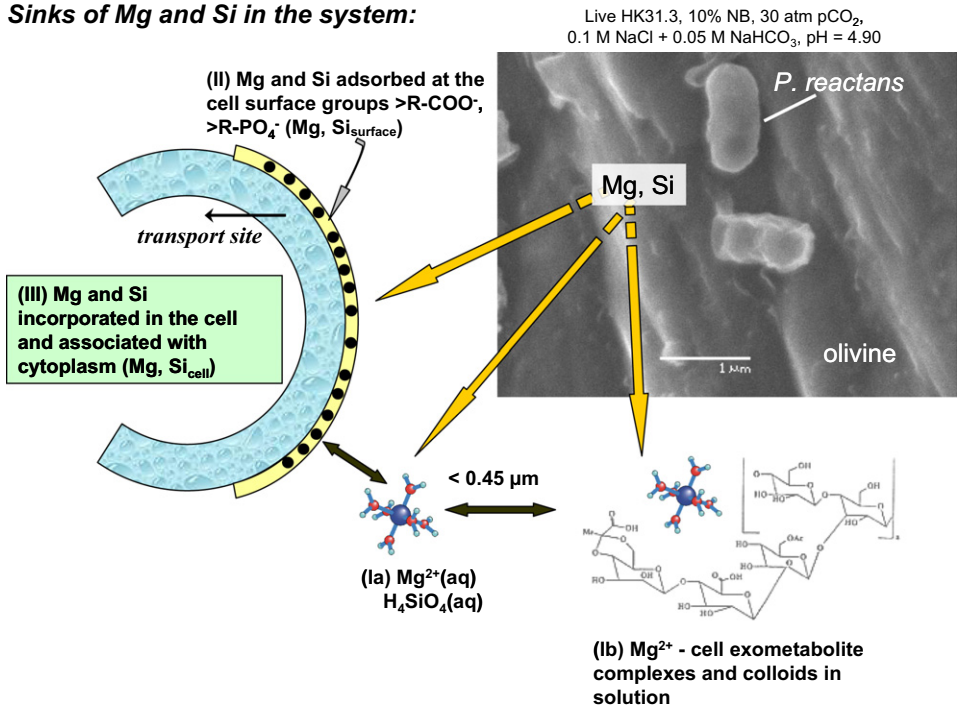

Fig. 14. Conceptual scheme of Mg and Si sources and sinks in the olivine – bacteria system.

occurring at the few atomic layers of the forsterite surface, the most surface layer of reacted forsterite can be seen as polymerized Si dimers connected with each other by common hydrogen-bonded water molecules and linked to the Mg octahedra deeper in the structure. As a result, the rate-limiting breaking of Mg–O bonds in Mg–O–Si units is weakly influenced by polarization capacity of adsorbed organic ligands. Moreover, bacterial organic polymers attached to the surface may partially hinder Mg hydration and bond polarization by water molecules.

The Si-rich, Mg-depleted layer becomes negligibly thin or disappears in neutral solutions. Therefore, one may expect a close-to-stoichiometric chemical composition of olivine surface in these conditions, as also confirmed by the X-ray Photoelectron Spectroscopy data (Pokrovsky and Schott, 2000b). In this region, therefore, the maximal effect of live bacteria and organic ligand occurs, via mainly polarization of Mg–O bonds due to adsorption on the surface.

In alkaline solutions, preferential Si removal from forsterite surfaces leads to formation of a Mg-rich layer (Pokrovsky and Schott, 2000a). The control of forsterite dissolution by the hydrolysis of Mg surface groups at pH $\geqslant$ 9 also accounts for its inhibition by dissolved carbonate via the formation of $>MgCO_3^-$ surface species on one (Pokrovsky and Schott, 2000b) or two (Wogelius and Walther, 1991) $>MgOH_2^+$ surface centers. It follows that $>MgOH_2^+$ moieties covered by adsorbed carbonate/bicarbonate ions form low reactive $>MgCO_3^-$, $>MgCO_3^\circ$ centers whose interaction with bacterial surfaces, exometabolites and exopolysaccharides, and organic ligands such as gluconate is weaker than that of «pristine» Mg–O–Si groups of olivine in neutral solution (pH 6). Indeed, the effect of various organic ligands on magnesite ($MgCO_3$) dissolution is rather weak (Jordan et al., 2007). This scheme also corroborates the results of other basic silicate dissolution in the presence of organic ligands such as diopside ($CaMgSi_2O_6$). This mineral is characterized by much weaker influence of carboxylate ligands on dissolution rate in alkaline solutions compared to that in neutral solutions, due mostly to negative mineral charge and electrostatic repulsion of ligands from mineral surface (Golubev and Pokrovsky, 2006). Enhanced effect of organic ligands on olivine dissolution with pH increase in acidic and circumneutral solutions has been also reported in previous studies (Hänchen et al., 2006; Olsen and Rimstidt, 2008). Note that the possibility of «passivation» of the olivine surface by $Fe(OH)_3$ in basic solutions is very unlikely at the conditions of this study: oxidation of Fe(II) into Fe(III) and Fe oxy(hydr)oxide precipitation should be significantly retarded by high concentration of dissolved organic matter (5–25 mg DOC/L, see González et al., 2011). Besides, organic ligand – enhanced dissolution of Fe oxy(hydr)oxides is much more efficient than that of $Mg(OH)_2$ and basic silicates, as a results, the newly-formed iron oxy(hydr)oxides will be rapidly dissolving in the presence of organic ligands.

4.4. Comparison with literature data on the effect of bacteria on silicate minerals dissolution

Over the past decades, extensive research has been done on the effect of organic ligands on mineral dissolution rate (see Ganor et al., 2009 for review). We do not anticipate any significant olivine rate increase in the presence of natural organic matter at the CO_2 sequestration site because of low concentration of total DOC (0.5–1.2 mg/L at the Hellisheidi site, Shirokova et al., 2009). Concentration of

small-size organic ligands in deep aquifers is certainly lower than that measured in soil solutions (1–50 μM, Jones, 1998; Van Hees et al., 2005). At these concentration of ligands, dissolution rates of other Mg(Ca)-bearing silicates similar to olivine such as diopside and wollastonite remain unaffected by the presence of dissolved organics (Golubev and Pokrovsky, 2006; Pokrovsky et al., 2009b).

In contrast to relatively good knowledge of organic ligands effect on basic silicate dissolution, the literature data on the effect of bacteria are rather scarce. For example, it has been shown that a soil strain of genera *Pseudomonas* is capable of producing 2-ketogluconic acid from glucose and thus dissolving Ca, Zn, Mg silicates, wollastonite, apophyllite and olivine via formation of Ca-2 ketogluconate (Webley et al., 1960; Duff et al., 1962, 1963); however, no quantitative parameters of the process were assessed. In contrast, a recent study of soil rhizospheric bacteria *Pseudomonas aureofaciens* does not reveal any significant effect of bacteria on wollastonite dissolution both in nutrient-free and nutrient-rich solutions (Pokrovsky et al., 2009b). Fayalite (Fe_2SiO_4) dissolution at pH = 2 in the presence of acidophilic, iron-oxidizing bacteria was significantly inhibited compared to abiotic controls (Santelli et al., 2001). This inhibition was attributed to formation of unreactive laihunite-like ($Fe^{2+}Fe^{3+}{}_2(SiO_4)_2$) surface region due to bacterial oxidation of released Fe^{2+} (Welch and Banfield, 2002). However, such mechanisms are unlikely to occur at the conditions of our experiments because of much higher pH values, and, as a result, significantly lower dissolved Fe concentration.

Aluminosilicates and Fe-bearing minerals are much more susceptible to microbial-driven dissolution compared to Ca, Mg-bearing orthosilicates. The main reason is the change of Al and Fe speciation in solution due to bacterial exometabolites and siderophores leading to a decrease of the activity of free Al^{3+} and Fe^{3+}, avoiding formation of secondary insoluble oxides and increase of the overall dissolution rate (Welch and Ullman, 1993; Vandevivere et al., 1994; Oelkers and Schott, 1998; Liermann et al., 2000; Maurice et al., 2001) or the selective uptake of trace metals (Brantley et al., 2001). Despite a common opinion that microbes accelerate weathering (Robert and Berthelin, 1986; Thorseth et al., 1992; Uroz et al., 2009), there are also studies that demonstrate rather weak or inhibiting effect (see for review Valsami-Jones and McEldowney, 2000; Hutchens, 2009; Sverdrup, 2009). Thus, biotite weathering in the presence of ectomycorrhizal fungus, *Suillus tomentosus*, demonstrated only weak or no effect compared to abiotic experiments (Balogh-Brunstad et al., 2008). Similar conclusion for this mineral has been reached in experiments with several typical bacterial and fungal strains (Hopf et al., 2009). Finally, dissolution of basaltic glass was negligibly affected by the presence of *P. reactans* (Stockman et al., 2010a,b).

4.5. Application to CO_2 underground sequestration scenarios and soil weathering

By encompassing the largest variety of bacterial live conditions, nutrient-rich and nutrient-free media, we explored two most extreme cases of heterotrophic bacterial impact on mineral dissolution. Typical concentrations of live cells used in present experiments is $(1–9) \times 10^8$ cell mL^{-1} in mixed-flow reactors and $\sim 10^7$–10^6 cell mL^{-1} in batch high-pCO_2 pressure reactors. This is significantly higher than the concentration of culturable heterotrophic bacteria measured in samples of Icelandic groundwaters used to separate *P. reactans* (40–520 CFU mL^{-1}, Shirokova et al., 2009). At the same time, our experimental concentrations are comparable with (i) average bacterial populations in soils that range between 10^6–10^9 cells cm^{-3} (Atlas and Bartha, 1993); (ii) bacterial concentrations in shallow aquifers (10^6 cells mL^{-1}, Ehrlich, 1996) and in deep subsurface environments (Sinclair and Ghiorse, 1989; Stevens and McKinley, 1995; Pedersen, 1997). For example, granite bedrock boreholes down to a maximum of 860 m contain in average 2.6×10^5 total bacteria mL^{-1} and 7.7×10^3 CFU (culturable bacteria) mL^{-1} (Pedersen and Ekendahl, 1990). It is known that culturable bacteria may only represent a small proportion of the species present (the ones that respond well to culture conditions), not necessarily the ones that had an important function in situ, with a possible bias towards rare species (e.g., Pedrós-Alió, 2006). Nevertheless, we believe that the very high concentrations of bacterial strain used in the present study should allow straightforward evaluation of the degree to which the heterotrophic bacteria are capable of influencing mineral dissolution in natural settings.

It follows from results of this study that the presence of carbonate/bicarbonate ions and alkaline solutions (pH $\geqslant$ 9), typical for basaltic aquifers should significantly inhibit the impact of heterotrophic microbial activity and cell exometabolites on olivine dissolution rate. In acidic, CO_2-saturated solutions at pH < 5 the impact of heterotrophic bacteria is also minor. Only in neutral, carbonate-free solutions do the live but starving cells and dissolved organic ligands measurably enhance olivine forward dissolution rates. This implies the existence of rather narrow window, in which the underground biota may actually affect basic silicate reactivity at the conditions of CO_2 storage. At the typical scenario of CO_2 sequestration in basaltic aquifers, initially acidic, CO_2-saturated solutions will be progressively replaced by neutral, HCO_3-bearing solutions. Note that in situ carbonate mineralization will decrease the concentration of dissolved inorganic carbon while maintaining the pH around 7. During this stage of CO_2 sequestration, one may expect a pronounced and positive effect of underground biota on mineral reactivity. Finally, in the post injection period, as the CO_2-rich front moves into the aquifer, pH increases to >7 following carbonates/silicates dissolution as shown by reactive transport simulations (Brosse, 2002; Knauss et al., 2005). At these pH values, the aqueous C-speciation changes from $H_2CO_3^*$ to HCO_3^- and CO_3^{2-} – dominated which should result in an inhibition of both olivine (Pokrovsky and Schott, 2000b) and carbonate mineral dissolution (Pokrovsky et al., 2005b, 2009a). An important conclusion is that aqueous bacteria and organic ligands are in no way capable preventing this drop in olivine and calcite dissolution rate as followed from results of the present study and that of Oelkers et al. (2011), respectively.

In a more general perspective, relatively weak effect of bacteria and microbial exometabolites on olivine (this study) and other Ca–Mg-bearing silicates such as wollastonite (Pokrovsky et al., 2009b) reactivity in aqueous solutions is that the impact of plants and biota on "basic" mineral chemical weathering in soils may be weaker than generally argued for (alumino)silicates. Indeed, the main factor controlling the aluminosilicates dissolution – aqueous activity of dissolution inhibitor Al^{3+}(aq) – is not important for Ca, Mg-bearing silicates since the far-from-equilibrium rates of the latter's are not controlled by the presence in solution of mineral constituents (Ca, Mg, and Si, at least in the neutral pH range, Schott et al., 2009). The complexation of organic ligands with aqueous and surface Al and complexation of Al with bacterial surface will be the main mechanisms of bacterial influence on aluminosilicates dissolution via aqueous Al^{3+} removal from solution thus decreasing its inhibiting effect and the supersaturation degree with respect to secondary Al-phases. In contrast, speciation of Ca and Mg in solution is weakly affected by the presence of biological ligands and the adsorption of organic matter on the surface of basic silicates is weak. As a result, the atmospheric CO_2 consumption on the land and Ca, Mg-associated transport of aqueous bicarbonate ions in rivers linked to basic silicates weathering is unlikely to be directly controlled by heterotrophic microbiological activity in soils.

5. CONCLUDING REMARKS

Experimental study of olivine reactivity in the presence of the heterotrophic bacterium *P. reactans* extracted from the basaltic aquifer CO_2 storage site was performed at a large variety of experimental conditions, both with nutrient-free and nutrient-rich media. These two extreme cases of bacterial metabolism together with a wide range of cell concentration (10^3–10^9 cell mL^{-1}) allowed exploring both active and passive mechanism of bacteria interaction with mineral surface under experimental conditions relevant to natural settings. Stoichiometric olivine dissolution rates measured in batch reactors at pH = 4.5, 30 atm pCO_2 and 25 °C yielded log R ranging from −12.4 to −12.8 mol/cm^2/s in agreement with previous measurements in CO_2-free systems. Long-term olivine dissolution rate at pH around 7 and atmospheric pCO_2 is only weakly affected by the presence of live bacteria, in agreement with previous results on wollastonite ($CaSiO_3$) dissolution rate in the presence of another gram-negative bacteria, *P. aureofaciens* (Pokrovsky et al., 2009b). Effect of *P. reactans* and their exometabolites on olivine dissolution at 25 °C, pH 6–9, 0.1 M NaCl, 0–0.01 M $NaHCO_3$ at naturally-relevant conditions is rather minor. Overall, this work demonstrates inhibiting rather than accelerating effect of heterotrophic bacterial activity on olivine reactivity under conditions of CO_2 storage.

ACKNOWLEDGEMENTS

We are grateful to anonymous reviewers for very constructive comments. This work was supported by the ANR program (National Agency for Research, within the framework of the CO2-FIX project under contract ANR-08-PCO2-003). The authors are grateful to A. Castillo and M. Thibaut for careful technical assistance with the B.E.T. and XRD analyses, respectively. T. Aigouy is thanked for assistance with the SEM analyses.

REFERENCES

Allison J. D., Brown D. S. and Novo-Gradac K. J. (1991) *MINTEAQA2/PRODEFA2, A Geochemical Assessment Model for Environmental Systems: Version 3.0 User's Manual*. U.S. EPA, Athens, GA, p. 106.

Aouad G., Crovisier J. L., Damidot D., Stille P., Hutchens E., Mutterer J., Meyer J. M. and Geoffroy V. (2008) Interactions between MSWI bottom ash and *Pseudomonas aeruginosa*. *Sci. Total Environ.* **393**(2–3), 385–393.

Atlas R. M. and Bartha R. (1993) *Microbial Ecology Fundamentals and applications*. Benjamin/Cummings, 563.

Awad A., Van Groos A. F. K. and Guggenheim S. (2000) Forsteritic olivine: effect of crystallographic direction on dissolution kinetics.. *Geochim. Cosmochim. Acta* **64**, 1765–1772.

Balogh-Brunstad Z., Keller K. C., Dickinson J. T., Stevens F., Li C. Y. and Bormann B. T. (2008) Biotite weathering and nutrient uptake by ectomycorrhizal fungus, *Suillus tomentosus*, in liquid-culture experiments. *Geochim. Cosmochim. Acta* **72**, 2601–2618.

Barker W. W., Welch S. A. and Banfield J. F. (1997) Biogeochemical weathering of silicate minerals. In Geomicrobiology: Interactions Between Microbes and Minerals (eds. J. F. Banfield, and K. H. Nealson). *Rev. Mineral.* 35, Mineralogical Society of America, pp. 391–428.

Bearat H., McKelvy M. J., Chizmeshya A. V. G., Gormley D., Nunez R., Carpenter R. W., Squires K. and Wolf G. H. (2006) Carbon sequestration via aqueous olivine mineral carbonation: role of passivating layer formation. *Environ. Sci. Technol.* **40**, 4802–4808.

Bennett P. C. and Casey W. H. (1994) Organic acids and the dissolution of silicates. In *The Role of Organic Acids in Geological Processes* (eds. E. D. Pittman and M. Lewan). Springer-Verlag, New York, pp. 162–201.

Blum A. and Lasaga A. (1988) Role of surface speciation in the low-temperature dissolution of minerals. *Nature* **331**, 431–433.

Brantley S. L., Liermann L., Bau M. and Wu S. (2001) Uptake of trace metals and rare earth elements from hornblende by a soil bacterium. *Geomicrobiol. J.* **18**, 37–61.

Brosse E., (ed.) (2002) Stockage de gaz acides dans les aquifères et les réservoirs pétroliers: les effets à long terme. Projet CEP and M G.7307/02 – Rapport Final IFP.

Chen Y. and Brantley S. L. (2000) Forsterite dissolution at 65 °C and 2 < pH < 5. *Chem. Geol.* **165**, 267–281.

Daval D., Martinez I., Corvisier J., Findling N., Goffé B. and Guyot F. (2009) Carbonation of Ca-bearing silicates, the case of wollastonite: experimental investigations and kinetic modeling. *Chem. Geol.* **265**, 63–78.

Daval D., Hellmann R., Corvisier J., Tisserand D., Martinez I. and Guyot F. (2010) Dissolution kinetics of diopside as a function of solution saturation state: macroscopic measurements and implications for modeling of geological storage of CO_2. *Geochim. Cosmochim. Acta* **74**, 2615–2633.

Davis K. J., Nealson K. H. and Lüttge A. (2007) Calcite and dolomite dissolution rates in the context of microbe–mineral surface interactions. *Geobiology* **5**, 191–205.

Duff R. B., Webley D. M. and Scott R. O. (1962) Solubilization of minerals and related materials by 2-ketogluconic acid-producing bacteria. *Soil Sci.* **95**, 105–114.

Edwards K. J., Bach W., McCollom T. M. and Rogers D. (2004) Neutrophilic iron-oxidizing bacteria in the ocean: their habitats, diversity, and roles in mineral deposition, rock alteration, and biomass production in the deep-sea. *Geomicrobiol. J.* **21**, 393–404.

Ehrlich H. L. (1996) *Geomicrobiology*. Marcel Dekker, Inc., New York, p. 719.

Eriksson E. (1982) On the dissolution rate of forsterite in aqueous solutions. *Vatten* **38**, 409–415.

Friis A. K., Davis T. A., Figueira M. M., Paquette J. and Mucci A. (2003) Influence of *Bacillus subtilis* cell walls and EDTA on calcite dissolution rates and crystal surface features. *Environ. Sci. Technol.* **37**, 2376–2382.

Fowle D. A. and Fein J. B. (2000) Experimental measurements of the reversibility of metal–bacteria adsorption reactions. *Chem. Geol.* **168**, 27–36.

Ganor J., Reznik I.J. and Rosenberg Y.O. (2009) Organics in water–rock interactions. In *Reviews in Mineralogy and Geochemistry, Thermodynamics and Kinetics of Water–Rock Interaction*, vol. 70 (eds. E. H. Oelkers and J. Schott), Mineralogical Society of America; St. Louis, MO: Geochemical Society pp. 259–369.

Garcia B., Beaumont V., Perfetti E., Rouchon V., Blanchet D., Oger P., Dromart G., Huc A.-Y. and Haeseler F. (2010) Experiments and geochemical modeling of CO_2 sequestration by olivine: potential, quantification. *Appl. Geochem.* **25**, 1383–1396.

Gérard E., Moreira D., Philippot P., Van Kranendonk M. J. and López-García P. (2009) Modern subsurface bacteria in pristine 2.7 Ga-old fossil stromatolite drillcore samples from the Fortescue Group, Western Australia. *PLoS ONE* **4**(4), e5298, doi:10.1371/ journal.pone.0005298.

Giammar D. E., Bruant R. G. and Peters C. A. (2005) Forsterite dissolution and magnesite precipitation at conditions relevant for deep saline aquifer storage and sequestration of carbon dioxide. *Chem. Geol.* **217**, 257–276.

Gislason S. R., Wolff-Boenisch D., Stefansson A., Oelkers E. H., Gunnlaugsson E., Sigurdardottir H., Sigfusson B., Broecker W. S., Matter J. M., Stute M., Axelsson G. and Fridriksson T. (2010) Mineral sequestration of carbon dioxide in basalt: a pre-injection overview of the CarbFix project. *Int. J. Greenhouse Gas Control* **4**, 537–545.

Golubev S. V. and Pokrovsky O. S. (2006) Experimental study of the effect of organic ligands on diopside dissolution kinetics. *Chem. Geol.* **235**, 377–389.

Golubev S. V., Bauer A. and Pokrovsky O. S. (2006) Effect of pH and organic ligands on the kinetics of smectite dissolution at 25 °C. *Geochim. Cosmochim. Acta* **70**, 4436–4451.

González A. G., Jimenez-Villacorta F., Shirokova L. S., Pokrovsky O. S., Santana-Casiano J. M., González-Dávila M. and Emnova E. E. (2011) Speciation of Fe adsorbed on soil and aquatic bacteria: XAS structural study. *Geophysical Research Abstracts,* EGU General Assembly 2011, **13,** EGU2011-7456.

Grandstaff D. E. (1978) Changes in surface area and morphology and the mechanism of forsterite dissolution. *Geochim. Cosmochim. Acta* **42**, 1899–1901.

Grandstaff D. E. (1986) The dissolution rate of forsteritic olivine from Hawaiiah beach sand. In *Rates of Chemical Weathering of Rocks and Minerals* (eds. S. M. Colman and D. P. Dethier). Elsevier Science Publishing Co Inc., Academic Press, pp. 41–57.

Grantham M. C., Dove P. M. and Dichristina T. J. (1997) Microbially catalyzed dissolution of iron and aluminum oxyhydroxide mineral surface coatings. *Geochim. Cosmochim. Acta* **61**, 4467–4477.

Hangx S. J. T. and Spiers C. J. (2009) Reaction of plagioclase feldspars with CO_2 under hydrothermal conditions. *Chem. Geol.* **265**, 88–98.

Hänchen M., Prigiobbe V., Storti G., Seward T. M. and Mazzotti M. (2006) Dissolution kinetics of forsteritic olivine at 90–150 °C including effects of the presence of CO_2. *Geochim. Cosmochim. Acta* **70**, 4403–4416.

Hänchen M., Krevor S., Mazzotti M. and Lackner K. S. (2007) Validation of a population balance model for olivine dissolution. *Chem. Eng. Sci.* **62**, 6412–6422.

Hochella, Jr., M. F. (1990) Atomic structure, microtopography, composition, and reactivity of mineral surfaces. In *Mineral-Water Interface Geochemistry*, 23M. F. Hochella Jr. and A. R. White. Rev. Mineral., pp. 87–132.

Hopf J., Langenhorst F., Pollok K., Merten D. and Kothe E. (2009) Influence of microorganisms on biotite dissolution: an experimental approach. *Chem. der Erde* **69**(S2), 45–56.

Hutchens E. (2009) Microbial selectivity on mineral surfaces: possible implications for weathering processes. *Fungal Biol. Rev.* **23**, 115–121.

Hutchens E., Valsami-Jones E., McEldowney S., Gaze W. and McLean J. (2003) The role of heterotrophic bacteria in feldspar dissolution – an experimental approach. *Mineral. Mag.* **67**(6), 1157–1170.

Hutchens E., Valsami-Jones E., Harouiya N., Chairat C., Oelkers E. H. and McEldoney S. (2006) An experimental investigation of the effect of *Bacillus megaterium* on apatite dissolution. *Geomicrobiol. J.* **23**, 177–182.

Johnson K. J., Ams D. A., Wedel A. N., Szymanowski J. E. S., Weber D. L., Schneegurt M. A. and Fein J. B. (2007) The impact of metabolic state on Cd adsorption onto bacterial cells. *Geobiology* **5**, 211–218.

Jones D. L. (1998) Organic acids in the rhizosphere – a critical review. *Plant Soil* **205**, 25–44.

Jordan G., Pokrovsky O. S., Guichet X. and Schmall W. (2007) Organic and inorganic ligand effects on magnesite dissolution at 100 °C and pH = 5 to 10. *Chem. Geol.* **242**, 484–496.

Knauer K., Behra R. and Sigg L. (1997) Effects of free Cu^{2+} and Zn^{2+} ions on growth and metal accumulation in freshwater algae. *Environ. Toxicol. Chem.* **16**, 220–229.

Knauss K., Johnson J. W. and Steefel C. I. (2005) Evaluation of the impact of CO_2, con-contaminant gas, aqueous fluid and reservoir–rock interactions on the geologic sequestration of CO_2. *Chem. Geol.* **217**, 339–350.

Kutuzova R. S. (1969) Release of silica from minerals as a result of microbial activity. *Mikrobiologiya* **38**, 714–721 (Engl. transl. pp. 596–602).

Le Faucher S., Behra R. and Sigg L. (2005) Thiol and metal contents in periphyton exposed to elevated copper and zinc concentrations: a field and microcosm study. *Environ. Sci. Technol.* **39**, 8099–8107.

Lee J.-U. and Fein J. B. (2000) Experimental study of the effects of *Bacillus subtilis* on gibbsite dissolution rates under near-neutral pH and nutrient-poor conditions. *Chem. Geol.* **166**, 193–202.

Lebedeva E. V., Lyalikova N. N. and Bugel'skii Y. Y. (1979) Participation of nitrifying bacteria in the weathering of serpentinized ultrabasic rocks. *Mikrobiologiya* **47**, 1101–1107 (Engl. transl. pp. 898–904).

Liermann L. J., Kalinowski B. E., Brantley S. L. and Ferry J. G. (2000) Role of bacterial siderophores in dissolution of hornblende. *Geochim. Cosmochim. Acta* **64**, 587–602.

Luce R. W., Bartlett R. W. and Parks G. A. (1972) Dissolution kinetics of magnesium silicates. *Geochim. Cosmochim. Acta* **36**, 35–50.

Lüttge A. and Conrad P. G. (2004) Direct observation of microbial inhibition of calcite dissolution. *Appl. Environ. Microbiol.* **70**, 1627–1632.

Malinovskaya I. M., Kosenko L. V., Votselko S. K. and Podgorskii V. S. (1990) Role of *Bacillus mucilaginosus* polysac-

charide in degradation of silicate minerals. *Mikrobiologiya* **59**, 70–78 (Engl. transl. pp. 49–55).

Martell A. E., Smith R. M. and Motekaitis R. J. (1997) *NIST Critically selected stability constants of metal complexes. Database software Version 3.0*. Texas A & M University, College Station, TX.

Matter J. M. and Kelemen P. B. (2009) Permanent storage of carbon dioxide in geological reservoirs by mineral carbonation. *Nat. Geosci.* **2**, 837–841.

Maurice P. A., Vierkorn M. A., Hersman L. E. and Fulghum J. E. (2001) Dissolution of well and poorly ordered kaolinites by an aerobic bacterium. *Chem. Geol.* **180**, 81–97.

Murphy W. M. and Helgeson H. C. (1987) Thermodynamic and kinetic constraints on reaction rates among minerals and aqueous solutions: III. Activated complex and the pH-dependence of the rates of feldspar, pyroxene, wollastonite, and forsterite hydrolysis. *Geochim. Cosmochim. Acta* **51**, 3137–3153.

Nazina T. N., Luk'yanova E. A., Zakharova E. V., Ivoilov V. S., Poltaraus A. B., Kalmykov S. N., Belyaev S. S. and Zubkov A. A. (2006) Distribution and activity of microorganisms in the deep repository for liquid radioactive waste at the Siberian chemical combine. *Microbiology* **75**(6), 727–738.

Nazina T. N., Luk'yanova E. A., Zakharova E. V., Konstantinova L. I., Kalmykov S. N., Poltaraus A. B. and Zubkov A. A. (2010) Microorganisms in a disposal site for liquid radioactive wastes and their influence on radionuclides. *Geomicrobiol. J.* **27**, 473–486.

Neaman A., Chorover J. and Brantley S. L. (2005a) Implications of the evolution of organic acid moieties for basalt weathering over geological time. *Am. J. Sci.* **305**, 147–185.

Neaman A., Chorover J. and Brantley S. L. (2005b) Element mobility patterns records organics ligands in soils on early Earth. *Geology* **33**, 117–120.

Neaman A., Chorover J. and Brantley S. L. (2006) Effects of organic ligands on granite dissolution in batch experiments at pH 6. *Am. J. Sci.* **306**, 451–473.

Oelkers E. H. (2001) An experimental study of forsterite dissolution kinetics as a function of temperature and aqueous Mg and Si concentration. *Chem. Geol.* **175**, 485–494.

Oelkers E. H. and Schott J. (1998) Does organic acid adsorption affect alkali-feldspar dissolution rates? *Chem. Geol.* **151**, 235–245.

Oelkers E. H., Golubev S. V., Charait C., Pokrovsky O. S. and Schott J. (2009) The surface chemistry of multi-oxide silicates. *Geochim. Cosmochim. Acta* **73**, 4617–4634.

Oelkers E. H., Golubev S. V., Pokrovsky O. S. and Bénézeth P. (2011) Do organic ligands effect calcite dissolution rates? *Geochim. Comsochim. Acta* **75**, 1799–1813.

Olsen A. A. and Rimstidt D. J. (2008) Oxalate-promoted forsterite dissolution at low pH. *Geochim. Cosmochim. Acta* **72**, 1758–1766.

Pedersen K. (1997) Microbial life in deep granitic rock. *FEMS Microbiol. Rev.* **20**, 399–414.

Pedersen K. and Ekendahl S. (1990) Distribution and activity of bacteria in deep granitic groundwaters of Southeastern Sweden. *Microb. Ecol.* **20**, 37–52.

Pedrós-Alió C. (2006) Marine microbial diversity: can it be determined? *Trends Microbiol.* **14**, 257–263.

Pokrovsky O. S. and Schott S. (2000a) Forsterite surface composition in aqueous solutions: a combined potentiometric, electrokinetic, and spectroscopic approach. *Geochim. Cosmochim. Acta* **64**, 3299–3312.

Pokrovsky O. S. and Schott J. (2000b) Kinetics and mechanism of forsterite dissolution at 25 °C and pH from 1 to 12.. *Geochim. Cosmochim. Acta* **64**, 3313–3325.

Pokrovsky O. S., Schott J. and Castillo A. (2005a) Kinetics of brucite dissolution at 25 °C in the presence of organic and inorganic ligands and divalent metals. *Geochim. Cosmochim. Acta* **69**, 905–918.

Pokrovsky O. S., Golubev S. V. and Schott J. (2005b) Dissolution kinetics of calcite, dolomite and magnesite at 25 °C and 0 to 50 atm pCO_2. *Chem. Geol.* **217**, 239–255.

Pokrovsky O. S., Golubev S. V. and Jordan G. (2009a) Effect of organic and inorganic ligands on calcite and magnesite dissolution rates at 60 °C and 30 atm pCO_2. *Chem. Geol.* **265**, 33–43.

Pokrovsky O. S., Shirokova L. S., Bénézeth P., Schott J. and Golubev S. V. (2009b) Effect of organic ligands and heterotrophic bacteria on wollastonite dissolution kinetics. *Am. J. Sci.* **309**, 731–772.

Prigiobbe V., Costa G., Baciocchi R., Hänchen M. and Mazzotti M. (2009a) The effect of CO_2 and salinity on olivine dissolution kinetics at 120 °C. *Chem. Eng. Sci.* **64**, 3510–3515.

Prigiobbe V., Costa G., Baciocchi R., Hänchen M. and Mazzotti M. (2009b) Analysis of the effect of temperature, pH, CO_2, pressure and salinity on the olivine dissolution kinetics. *Energy Procedia* **1**, 4881–4884.

Robert M. and Berthelin J. (1986) Role of biological and biochemical factors in soil mineral weathering. In *Interactions of soil minerals with natural organics and microbes* (eds. P. M. Huang and M. Schnitzer). SSSA special publication 17, Wisconsin, pp. 453–495.

Rosso J. J. and Rimstidt J. D. (2000) A high resolution study of forsterite dissolution rates. *Geochim. Cosmochim. Acta* **64**, 797–811.

Sanemasa I., Yoshida M. and Ozawa T. (1972) The dissolution of forsterite in aqueous solutions of inorganic acids. *Bull. Chem. Soc. Jpn.* **45**, 1741–1746.

Santelli C. M., Welch S. A., Westrich H. R. and Banfield J. F. (2001) Fe oxidizing bacteria and the weathering of Fe silicate minerals. *Chem. Geol.* **180**, 99–115.

Schott J. and Berner R. A. (1983) X-ray photoelectron studies of the mechanism of iron silicate dissolution during weathering. *Geochim. Cosmochim. Acta* **47**, 2233–2240.

Schott J. and Berner R.A. (1985) Dissolution mechanisms of pyroxenes and olivines during weathering. In *The Chemistry of Weathering* (ed. J.J. Drever). Springer-Verlag, New York, LLC (NATO Science Series C), D. Riedel Publ. Co, 35–53.

Schott J., Pokrovsky O. S. and Oelkers E. H. (2009) The link between mineral dissolution/precipitation kinetics and solution chemistry: In *Reviews in Mineralogy & Geochemistry, Thermodynamics and Kinetics of Water–Rock Interaction*, vol. 70 (eds. E. H. Oelkers and J. Schott). Mineralogical Society of America; St. Louis, MO: Geochemical Society pp. 207–258.

Shirokova L. S., Bénézeth P. and Pokrovsky O. S. (2009) Effect of heterotrophic bacteria extracted from groundwater on Ca silicate dissolution. Proceedings of 19th Annual V.M. Goldschmidt Conference, Davos, Switzerland, 21–26 june 2009. *Geochim. Cosmochim. Acta* **73**(No. 13, Suppl. S), p. A1213.

Siegel D. I. and Pfannkuch H. O. (1984) Silicate mineral dissolution at pH 4 and near standard temperature and pressure. *Geochim. Cosmochim. Acta* **48**, 197–201.

Siever R. and Woodford N. (1979) Dissolution kinetics and the weathering of mafic minerals. *Geochim. Cosmochim. Acta* **43**, 717–724.

Sinclair J. L. and Ghiorse W. C. (1989) Distribution of aerobic-bacteria, protozoa, algae, and fungi in deep subsurface sediments. *Geomicrobiol. J.* **7**, 15–31.

Slaveykova V. I. and Wilkinson K. J. (2002) Physicochemical aspects of lead bioaccumulation by *Chlorella vulgaris*. *Environ. Sci. Technol.* **36**, 969–975.

Smiejan A., Wilkinson K. J. and Rossier C. (2003) Cd bioaccumulation by a freshwater bacterium, *Rhodospirillum rubrum*. *Environ. Sci. Technol.* **37**, 701–706.

Sorai M., Ohsumi T., Ishikawa M. and Tsukamoto K. (2007) Feldspar dissolution rates measured using phase-shift interferometry: implications to CO_2 underground sequestration. *Appl. Geochem.* **22**, 2795–2809.

Stevens T. O. and McKinley J. P. (1995) Lithoautotrophic microbial ecosystems in deep basalt aquifers. *Science* **270**, 450–454.

Stockmann G. J., Shirokova L. S., Pokrovsky O. S., Oelkers E. H., Bénézeth P. (2010a) Does the presence of bacteria effect basaltic glass dissolution rates? 1: Dead *Pseudomonas reactans*. *Geophysical Research Abstracts*, EGU General Assembly 2010, **12,** EGU2010-4420-2.

Stockmann G.J., Shirokova L.S., Pokrovsky O.S., Oelkers E.H., Bénézeth P. (2010b) Does the presence of bacteria affect basaltic glass dissolution rates? 2: Live *Pseudomonas reactans*. Goldschmidt Conference, Knoxville, USA, June 13-18, 2010. *Geochim. Cosmochim. Acta,* **74(11),** A995.

Sverdrup H. (1990) *The Kinetics of Base Cation Release due to Chemical Weathering*. Lund University Press, Lund, Sweden p. 245.

Sverdrup H. (2009) Chemical weathering of soil minerals and the role of biological processes. *Fungal Biol. Rev.* **23**, 94–100.

Sverdrup H. and Bjerle I. (1982) Dissolution of calcite and other related minerals in aqueous solutions in a pH-stat. *Vatten* **38**, 59–73.

Thorseth I. H., Furnes H. and Heldal M. (1992) The importance of microbiological activity in the alteration of natural basaltic glass. *Geochim. Cosmochim. Acta* **56**, 845–850.

Ullman W. J., Kirchman D. L., Welch S. A. and Vandevivere Ph. (1996) Laboratory evidence for microbially mediated silicate mineral dissolution in nature. *Chem. Geol.* **132**, 11–17.

Uroz S., Calvaruso Ch., Turpault M.-P. and Frey-Klett P. (2009) Mineral weathering by bacteria: ecology, actors and mechanisms. *Trends Microbiol.* **17**, 378–387.

Urrutia Mera M., Kemper M., Doyle R. and Beveridge T. J. (1992) The membrane-induced proton motive force influences the metal binding ability of *Bacillus subtilis* cell walls. *Appl. Environ. Microbiol.* **58**, 3837–3844.

Valsami-Jones E. and McEldowney S. (2000) Mineral dissolution by heterotrophic bacteria: principles and methodologies. In *Environmental Mineralogy: Microbial Interactions, Anthropogenic Influences, Contaminated Land and Waste Management* (eds. J. D. Cotter-Howells, L. S. Campbell, E. Valsami-Jones and M. Batchelder). Mineralogical Society of Great Britain & Ireland, pp. 27–55 (Special Series, 9).

Van Hees P. A. W., Jones D. L., Jentschke G. and Godbold D. L. (2005) Organic acid concentrations in soil solution: effect of young coniferous trees and ectomycorrhizal fungi. *Soil Biol. Biochem.* **37**, 771–776.

Vandevivere P., Welch S. A., Ullman W. J. and Kirchman D. L. (1994) Enhanced dissolution of silicate minerals by bacteria at near-neutral pH. *Microb. Ecol.* **27**, 241–251.

Webley D. M., Duff R. B. and Mitchell W. A. (1960) Plate method for studying the breakdown of synthetic and natural silicates by soil bacteria. *Nature* **188**, 766–767.

Webley D. M., Henderson E. K. and Taylor I. F. (1963) Microbiology of rocks and weathered stones. *J. Soil Sci.* **14**, 102–112.

Welch S. A. and Banfield J. F. (2002) Modification of olivine surface morphology and reactivity by microbial activity during chemical weathering. *Geochim. Cosmochim. Acta* **66**, 213–221.

Welch S. A. and Ullman W. J. (1993) The effect of organic acids on plagioclase dissolution rates and stoichiometry. *Geochim. Cosmochim. Acta* **57**, 2725–2736.

Welch S. A. and Ullman W. J. (1999) The effect of microbial glucose metabolism on bytownite feldspar dissolution rates between 5 and 35 °C. *Geochim. Cosmochim. Acta* **63**, 3247–3259.

Welch S. A. and Vandevivere P. (1994) Effect of microbial and other naturally occurring polymers on mineral dissolution. *Geomicrobiol. J.* **12**, 227–238.

Welch S. A., Barker W. W. and Banfield J. F. (1999) Microbial extracellular polysaccharides and plagioclase dissolution. *Geochim. Cosmochim. Acta* **63**, 1405–1419.

Westrich H. R., Cygan R. T., Casey W. H., Zemitis C. and Arnold G. W. (1993) The dissolution kinetics of mixed-cation orthosilicate minerals. *Am. J. Sci.* **293**, 869–893.

Wogelius R. A. and Walther J. V. (1991) Forsterite dissolution at 25 °C: effects of pH, CO2, and organic acids. *Geochim. Cosmochim. Acta* **55**, 943–954.

Wogelius R. A. and Walther J. V. (1992) Forsterite dissolution kinetics at near-surface conditions. *Chem. Geol.* **97**, 101–112.

Wu L., Jacobson A. D., Chen H.-C. and Hausner M. (2007) Characterization of elemental release during microbe-basalt interactions at T = 28 °C. *Geochim. Cosmochim. Acta* **71**, 2224–2239.

Wu L., Jacobson A. D. and Hausner M. (2008) Characterization of elemental release during microbe-granite interactions at T = 28 °C. *Geochim. Cosmochim. Acta* **72**, 1076–1095.

Associate editor: Roy A. Wogelius